Nonlinear Acoustic Method for Gas Bubbles Identification in Marine Sediments

by

Songhua Zhang

M.Eng. Wuhan University, 2002

A Thesis Submitted in Partial Fulfillment of the

Requirements for the Degree of

MASTER OF SCIENCES

In the School of Earth and Ocean Sciences

Nonlinear Acoustic Method for Gas Bubbles Identification in Marine Sediments

by

Songhua Zhang

M.Eng. Wuhan University, 2002

Supervisory Committee

Dr. Ross Chapman, School of Earth and Ocean Sciences

Supervisor

Dr. Stan Dosso, School of Earth and Ocean Sciences

Co-supervisor or Departmental Member

Departmental Member

Dr. Adam Zielinski, Department of Electrical and Computer Engineering

Outside Member

Dr. Jaroslaw Tegowski, Institute of Oceanology, Polish Academy of Sciences

Additional Member

Supervisory Committee

Dr. Ross Chapman, School of Earth and Ocean Sciences
Supervisor
Dr. Stan Dosso, School of Earth and Ocean Sciences
Co-supervisor or Departmental Member

Departmental Member
Dr. Adam Zielinski, Department of Electrical and Computer Engineering
Outside Member
Dr. Jaroslaw Tegowski, Institute of Oceanology, Polish Academy of Sciences
Additional Member

ABSTRACT

It is well known that gases are present in marine sediments. The gas found in the surficial layer of marine sediments is mostly due to biological origin or migration from deposits in deeper layers. A nonlinear acoustic remote sensing technique based on the nonlinear acoustic scattering theory of gas bubbles is introduced in this thesis to identify the gas bubbles in surficial layers of marine sediments and measure their concentrations. Two close transmitting frequencies were used to generate a nonlinear scattering effect from the gas bubbles in the sediments, and the nonlinear responses were generated only by gas bubbles instead of by other scatters in the sediments. An acoustic inversion was implemented on the nonlinear response, together with calibration results and scattering volume, to determine gas bubble concentrations. Results from the data collected at Gulf of Gdansk demonstrate that the nonlinear acoustic method is advantageous over other acoustic remote sensing methods in gas bubble identification and measurement, and provides more valuable information for seabed classification.

Table of Contents

List of Tables

List of Figures

Acknowledgments

First of all I would like to thank my supervisor Dr. Ross Chapman for his patient guidance, unremittent support and encouragement throughout my master program. Without his knowledge, perceptiveness and passion, I would not be able to finish this thesis. I would like to thank Dr. Jaroslaw Tegowski for his generous help in the nonlinear acoustic theory and great assistance in the project through the emails. I am also grateful for Dr. Stan Dosso and Dr. Adam Zielinski for their valuable suggestions on my research work. I would like to thank everyone in the ocean acoustics group for a very nice and friendly working environment and the helpful discussions. Last but not the least, I want to thank my parents, for their supports always behind me in every aspect.

Chapter 1

Introduction

It is well known that gases are present in marine sediments. There are many sources which give rise to their presence, such as gases produced during early diagenesis from biogenic degradation of organic matter; gases diffusing upward from depth where it has been produced by the thermo-catalytic cracking of more complex organic compounds; gases produced by submarine volcanic or geothermal processes; atmospheric gases originally dissolved in sea water. However, the most important mechanism for generating gas in the marine sediment is the microbial degradation of organic matter (Kaplan 1974).

The gas found in the surficial layer of marine sediments is most commonly due to one of two sources. One source is the biological origin, where the gas is formed by bacterial reduction of organic matter, and is composed mostly of methane. The other source is the product of migration out of deeper layers from hydrocarbons or clathrate deposits, which may contain methane and higher hydrocarbons.

The physical state of the gases in sediments can be either dissolved in the interstitial water or exist as free gas bubbles. It can also exist in a solid form as gas hydrates under specific conditions of high pressure and low temperature.

Knowledge about the gas presence, distribution and concentration in the ocean sediments can be very useful for many applications.

Firstly, information on bubble distribution and abundance is important in understanding the factors that control the formation, migration and distribution of shallow gas deposits.

Gassy sediments are very compressible and may suffer from reduced shear strengths due to certain combinations of seabed confining pressures. Therefore, the knowledge of the content and the structure of gas pockets contained a soil is essential for a good foundation design.

The presence of gas is also important in offshore hydrocarbon exploration. Serious blowouts have occurred during drilling, when the penetration of layers of gas-charged sediments has caused sudden buoyancy. Research into gas detection in sediments may provide a measure of safety for those involved in locating submerged oil and gas by a wise choice of siting of seabed structures, and the drilling operations.

The gas in the ocean sediments can also affect the marine environment, such as the animals and plants living at the bottom of a sea, by changing the seawater chemistry and forming dead areas in the water. It may also affect atmospheric carbon dioxide and methane levels. Obtaining information on gas distribution and abundance is necessary to determine the impact of this gas on the global environments and for the ecological control of the environment.

Although the fact that gases exist in marine sediments has been known for a long time, and the knowledge of the presence, composition and distribution of marine gases can lead to many useful applications nowadays, before the 1970s the investigation of these marine gases received little attention (Kaplan 1974). Early studies were almost exclusively directed toward bay or estuarine environments, and were essentially extensions of similar work undertaken on soil, swamps, and lakes. Much of the reliable work on shallow water marine

environments was under-taken by Koyama et al. at Nagoya University (Koyama 1953). The first successful attempt to obtain quantitative data in deeper water sediments was made by Emery and Hoggan (1958). They captured sediments in a core barrel that was capped and taken to the laboratory for gas removal and analysis by mass spectroscopy. From their analytical method, they were able to detect methane and several other volatile homologs. Although their techniques could not yield accurate data, as a first approximation, the results they obtained for shelf sediments off southern California are still valid. Subsequent studies by Reeburgh (1969) and others have produced quantitative data for specific gases in specific environments.

In the past few decades, the interest in gas bearing seabed sediments has been generated largely through the work of the oil industry, in geotechnical applications for foundation design of offshore structures, and the exploration and extraction of oil and gas.

The conventional methods employed for data collection on gas presence and concentration in sediments, which are described above, normally involve drilling or coring. These operations are tedious, inefficient, and costly. Besides, they produce sparse data. As a comparison, remote sensing techniques can provide the needed information for detecting, surveying, and measuring gas-bearing sediments at a much lower cost with acceptable accuracy and over a large area.

For instance, seismic remote sensing methods are used for monitoring of gas activities, based on the analysis of echo arrival time, echo intensity and phase variations. High power, low frequency sources are used for deep bottom penetration; while high frequency sources, both single beam and multi-beam, are used for bottom characterization based on wave scattering at the water-bottom boundary.

Another important example is the acoustic remote sensing methods, which are also employed for recognition of the presence of shallow gas concentrations. Due to changed acoustic properties of gas-saturated sediments, the shallow gas concentrations can be easily recognized by acoustic techniques.

However, compared to the research efforts in acoustic properties of water containing gas bubbles (Hampton and Anderson 1974), relatively few studies have been directed to the acoustic properties of bubbles in sediments. It is known that gas bubbles in water can vibrate and they have a fundamental resonance. Both the scattering cross section of a bubble and the attenuation by a bubble screen are maximum at resonance. Thus water containing bubbles is a highly dispersive propagation medium for frequencies near the fundamental resonance frequency of the bubbles.

In the same way, gas controls the acoustical properties of sediment at frequencies near the resonance frequency of the bubbles (Anderson 1980). When gas bubbles are present in sediments, even in small amounts, they can dominate the acoustic characteristics of the sediments (Boyle 1995). The attenuation values of gassy sediments are reported to be significantly larger than the values for saturated sediments (Nyborg *et al.* 1950). Sound speed is reported to be both decreased and increased when gas bubbles are present in sediments. The reason may be the degree to which bubbles in sediments act as a resonant system, and the relation of the sound frequency to the resonance frequency of the bubble (Anderson 1980). Most studies of acoustic properties of sediments have been conducted in shallow water areas, and very little has been published on the acoustical properties of sediments in the deep ocean which are known to contain gas, among which a notable paper describes anomalously high sound speeds in a gassy layer of sediment in 3600m of water depth (Stoll *et al.* 1971). The high value

of sound speed is attributed to the probable presence of gas in the form of a gas hydrate.

Given the knowledge of acoustic properties of the gassy sediments, acoustic remote sensing methods can be used for detecting gas bubbles in sediments. But significant ambiguity can exist between the acoustic backscattering signals from gas concentrations and other types of scatters. For instance, a hard rock interface can resemble a pocket of trapped gas. This introduces uncertainty into acoustic methods of gas concentration measurements and sediment classification. Finding an effective way of distinguishing gas bubble acoustic returns from other types of scatters is therefore critical.

One way of identifying bubble backscattering is to ensonify the sediment with a parametric signal and measure the scattered acoustic waves at combination frequencies. This procedure has been successfully employed to detect bubbles in the water column (Leighton *et al.* 1991), and also in medical sciences (Eatock *et al.* 1985). This nonlinear method is attracting increasing attention in bubble diagnostics. The problem of identifying gas bubbles trapped within sediment pores is considerably more complicated than that involving bubbles in the water column. Klusek *et al.* (1995) have explored the nonlinear acoustic properties of gas bubbles in sediments.

It is known that a gas bubble has prominent nonlinear properties. Nonlinear distortions in scattered fields from a bubble are easily observed at the second or higher harmonics of the incident frequency, the fundamental frequency, as well as at the sum and the difference frequencies of the primary waves (Zabolotskaya 1972). When two primary acoustic waves of different frequencies are incident upon a bubble, the interaction will generate both linear and nonlinear acoustic waves from the oscillating gas bubble. The existence of the nonlinear response

suggests the possibility of a new remote sensing technique, the nonlinear acoustic detection technique. Since nonlinear scattering from a bubble is much stronger than that from other scatterers in the sediments, the nonlinear acoustic detection technique provides the advantage of high selectivity of gas bubble returns, which distinguishes a bubble from the other scatterers. Different nonlinear acoustical methods have been developed for gas bubble diagnostics: the second harmonic method (Ostrovsky 1983); the difference and the sum frequency method (Zverev *et al.* 1980); the modulation method (Newhouse *et al.* 1984); the subharmonic method (Eller *et al.* 1969), the subharmonic-modulation method (Leighton 1996).

Since the bubble is an oscillator, the amplitude of the generated nonlinear frequency signal is developed through a resonance effect, which means only the resonant bubbles can be detected, because the amplitude of the scattered signal away from the bubble resonance is very small. Therefore, if the detection of bubbles of different sizes is required, one has to use several different frequencies in a bubble counter. This can be done by keeping the frequency of one of primary acoustic beams constant and then changing the other beam frequency.

This thesis work is related to the project of Gas Bubble Identification in Ocean Bottom Sediments Using a Non-linear Acoustic Method (GABI). Participating institutions includes Institute of Oceanology of the Polish Academy of Sciences (IOPAS) and University of Victoria. The team from IOPAS participated in the field experiments and provided experimental data, and team from University of Victoria took part in the data analysis and the interpretation of the results.

The project introduces a novel method of detecting gas bubbles in ocean sediments, in which high intensity acoustic sources are used to induce a non-

linear response from a gas bubble. This response in the form of echoes generated by bubbles is related to the gas bubble presence and concentration. Theoretical studies and limited experimentation have demonstrated the validity of this concept.

The main objective of the project is the design and demonstration of a non-linear acoustic system for the surveying and monitoring of shallow water and continental shelf sediments to detect gas bubbles. The project also intends to show this non-linear detection method to have many advantages over existing methods for ocean bottom surveying and monitoring of gas in sediments.

Specific project objectives include:

- development of an innovative non-linear method for acoustic remote sensing to better recognize the free gas concentration in the sediments;
- design of appropriate post processing algorithms for analysis of the acoustic data, to provide better recognition of bottom sediments;
- application of new geo-acoustic models, in particular models for seabed parameters derived from non-linear acoustic properties;
- work within the frame of a Geographical Information Systems (GIS) for handling the environmental information and the data set.

The major goal of this thesis work is to apply this novel nonlinear acoustic method to some data collected in the Baltic Sea to identify the gas bubbles location and concentration in the sediments, and confirm the validity of this nonlinear acoustic detecting method. The specific work done in the thesis includes:

- a data processing method for the data collected at Gdansk Bay;
- an inversion software package to invert the extracted nonlinear response to obtain bubble concentration;

- application of data processing procedure and inversion programs to selected data from J. Tegowski;
- interpretation of the results of data processing & inversion process in terms of bubble concentration;
- related results of bubble densities with the specific sediment type around Gdansk Bay.

This thesis is organized as follows: Chapter 2 presents the theory for the non-linear detection method; Chapter 3 describes the experimental setup for the nonlinear measurement systems; Chapter 4 states the data processing procedures, results at each data processing stage, and interpretation of final inversion results of bubble concentration; Chapter 5 gives the conclusion of this nonlinear acoustic remote sensing method for bubble identification in ocean sediments.

Chapter 2

Theory

This chapter outlines the theory as the background of the thesis work. Firstly the linear scattering properties of bubbles in water, which is well developed, will be introduced. Based on linear scattering theory of bubbles in water, the process of nonlinear scattering by the gas bubbles in sediments will be presented, which is the basis for experimental design and data processing of the nonlinear acoustic methods described in the following chapters.

2.1 Linear Scattering by a Single Ideal Bubble

The basic theory of linear bubble scattering properties will be reviewed in this sector. The review starts with the Rayleigh's model which describes the bubble behavior in the field of an acoustic wave. Then two key features of bubble dynamics will be discussed, bubble resonance and bubble damping, since they determine bubble behaviors at the scattering process. As a measurement of scattering efficiency, the scattering cross section of bubbles will later be discussed with its physical implications.

2.1.1 Theoretical Model

Lord Rayleigh (1917) described the first theoretical model of the gas bubble oscillations placed in the field of the acoustical wave, neglecting the effect of the surface tension. The equation of motion for the bubble radius is

$$R \cdot \ddot{R} + \frac{3}{2}\dot{R}^2 = \frac{P - P_\infty}{\rho}, \tag{2.1}$$

where R – bubble radius;

P – pressure inside bubble;

ρ - density of fluid;

P_∞ - pressure of surrounding fluid in the static situation or in the far distance from the bubble wall.

There are two methods in the literature that are used for describing the gas bubbles oscillations, and they are both based on the Rayleigh equation. The first method uses small radius changes in the Rayleigh equation (Prosperetti 1974) and it was improved after adding surface tension, viscous loss, pressure of the stream inside the bubble etc. (Tegowski 2004). The second method was proposed by Zabolotska and Soluyan (1972), which used the change of volume in the Rayleigh equation. The result of this manipulation is the equation describing oscillations of bubble volume. Both approaches are consistent for bubbles with radius greater than 10μm and for pressure of incident wave less than 0.1 of the equilibrium pressure of the medium.

2.1.2 Bubble Resonance

A very basic and important aspect of bubble scattering in different media is the bubble resonance. This fact reveals that gas bubbles in different media are capable of vibratory motion with a sharply peaked resonance at the fundamental

pulsation frequency. Such motion of the medium in the vicinity of a bubble is controlled by the internal pressure, which varies inversely with bubble volume. The gas bubble then acts as the cavity and the surrounding medium as the vibrating mass of an acoustical oscillator.

For bubbles in water, the resonance frequency is often described by a modified version of Minnaert's equation

$$f_0 = \frac{1}{2\pi r_0}\sqrt{\frac{3\gamma P_0}{A\rho_w}} \tag{2.2}$$

where γ - the ratio of specific heats of gas;

A - the polytropic coefficient;

r_0 - the equilibrium bubble radius;

P_0 - the equilibrium pressure at the bubble surface.

This expression is valid for calculating the resonance frequency of bubbles with radius greater than 10^{-3} cm, for $A = 1$ in the adiabatic region in water, $A = \gamma$ in the isothermal region, and a complete expression of A should be used for the transition region (Anderson 1980).

Similarly with the resonance of a gas bubble in water, gas bubbles in materials with nonzero shear modulus are also capable of resonant vibratory motion. In this case the surrounding material acts as the vibrating mass, analogous to the surrounding water mass for bubbles in water.

At least two lines of investigation of gas bubble resonance in solids have occurred: 1) taking bubbles as empty cavities, such as in geophysical studies (Blake 1952); 2) including the effects of the gas filling the cavity, such as in bioacoustic studies (Andreeva 1964).

For gas bubble in materials with nonzero shear modulus, Blake (1952) obtains an expression for the specific acoustic radiation impedance. The radiation

impedance of an empty cavity in a solid is the ratio of the pressure to the particle velocity at the bubble surface. Gas bubble resonance occurs when the reactive component, the imaginary part of the radiation impedance, is zero.

The resonance frequency of a bubble in the medium with nonzero shear modulus is given by

$$f_0 = \frac{1}{2\pi r}\sqrt{\frac{4G(1-\nu)}{-\rho_s(1-3\nu)}} \tag{2.3}$$

where G - Lamé parameters of the solid;

ρ_S - density of the solid;

ν - Poisson's ratio of the solid;

r - bubble (cavity) radius.

For $\nu < 1/3$, f_0 is imaginary, and the radiation reactance is negative, while the material with nonzero shear modulus is acting as a spring for all frequencies and there is no resonance; for $\nu = 1/3$, f_0 is infinite; for $1/3 < \nu < 1/2$, a resonance frequency above which the reactance is positive or inertial, while the solid is acting as a mass; for $\nu = 1/2$, the resonance frequency reduces to

$$f_0 = \frac{1}{2\pi r}\sqrt{\frac{4G}{\rho_s}}. \tag{2.4}$$

As known $\nu = 1/2$ is the limit value for a liquid or an incompressible material, and Eq. (2.4) has the similar form compared to Eq. (2.2), which describes the resonance frequency for bubble in water.

Andreeva (1964) includes the effects of gas in the boundary conditions and gives the following expression for the fundamental pulsation frequency of a gas bubble in fish tissue

$$f_0 = \frac{1}{2\pi r}\sqrt{\frac{(4G + 3\gamma P_0)}{\rho_s}}. \tag{2.5}$$

Thus the complete expression for the resonance frequency of a bubble, in a material with nonzero shear modulus, includes Minnaert's expression for the resonance frequency of a gas bubble in water modified by the elastic properties of such material (Anderson 1980).

2.1.3 Bubble Damping

The pulsation of bubbles in water is not loss-free, and the bubble damping is another important aspect of gas bubble dynamics. The motion of air bubbles in water is considered to be set into the spherical pulsation by a sound field with a specific frequency ω and a pressure amplitude. The damping constant d is defined in relation to the damping coefficient b as

$$d = \omega b / K_b \tag{2.6}$$

where K_b is the stiffness of the bubble (Anderson 1980). The damping constant can be written as a sum of the thermal constant, radiation constant, and viscous damping constant. Expressions for these three damping constants are given by Eller (1970), from which it can be derived that: 1) below resonance, thermal damping dominates; 2) above resonance, radiation damping dominates; 3) near resonance, there is a transition region from predominately thermal damping to predominately viscous damping. The damping constant is significantly different for bubbles at and off resonance.

Analogous to bubbles in water, damping of bubble pulsation in a solid consists of radiation, thermal, and viscous (internal friction) damping. Radiation damping results from energy radiated into the surrounding solid; while thermal damping results from heat energy conducted from the gas in a bubble during

compression; and internal friction in the solid surrounding the bubble is another loss mechanism.

The expression of damping constant both at and off resonance for a bubble in a solid is given as

$$d_s = \frac{1}{Q} = \frac{1}{Q_r} + \frac{1}{Q_t} + \frac{1}{Q_f} \tag{2.7}$$

where Q is the reciprocal specific dissipation function. The difference of the damping at and off resonance lies in the different expressions for individual terms of radiation damping constant Q_r, thermal damping constant Q_t, and internal friction damping constant Q_f (Anderson 1980).

2.1.4 Scattering Cross Sections

The efficiency of a scatterer is usually characterized by its scattering cross section σ_S, which is defined as the ratio of total acoustical power scattered by the scatterer over all directions W_S to the incident wave intensity I_i. Based on this definition, when the small bubble is insonified by a plane wave, the total acoustical scattering cross section is

$$\sigma_S(f) = \frac{W_S}{I_i} = 4\pi R^2 \frac{I_S}{I_i} = \frac{4\pi R^2 (P_S^2 / \rho_A c)}{(P_i^2 / \rho_A c)} \tag{2.8}$$

where R is the distance from the centre of the bubble to an arbitrary point in the medium; I_S is the scattered wave intensity; P_S and P_i are scattered and incident wave pressure respectively.

If an air bubble is of radius a, which is small compared with the wavelength λ, is insonified by a plane wave of frequency ω, the sound wave pressure at the bubble is

$$p_i = A\exp(-i\omega t). \tag{2.9}$$

The incident wave gives rise to pulsations of the bubble which will generate a spherical scattered wave in the surrounding medium. The scattered acoustic pressure in the medium can be written as

$$p_S = (B/R)\exp[i(kR-\omega t)] \tag{2.10}$$

where B is the unknown amplitude determined from the boundary conditions at the bubble surface, and k is the wave number. For $ka \ll 1$, B can be written as (Brekhovskikh *et al.* 1991)

$$B = \frac{aA}{[(f_0/f)^2 - 1 - ika]}. \tag{2.11}$$

Then the field of the scattered wave can be determined. Its amplitude reaches maximum when the incident wave frequency is equal to the resonance frequency of the bubble. The term ika in (2.11) is due to the radiation losses during the bubble oscillations.

From Eq. (2.8) we can obtain the scattering cross section

$$\sigma_S(f) = \frac{4\pi a^2}{[(f_R/f)^2 - 1]^2 + (ka)^2} \qquad (ka < 1). \tag{2.12}$$

To understand the physical meaning of σ_S, we rewrite (2.8) in the form

$$4\pi R^2 I_S = \sigma_S I_i. \tag{2.13}$$

This indicates that the acoustic power scattered by a bubble over all directions is equal to that transferred by an incident wave through the surface σ_S normal to the direction of the incident wave.

In Fig.2.1 the ratio of the scattering cross section to the purely geometrical cross section for a sphere of radius a, represented as $\sigma_S/(\pi a^2)$, is shown as a function of ka. The peak corresponds to the resonance value of ka.

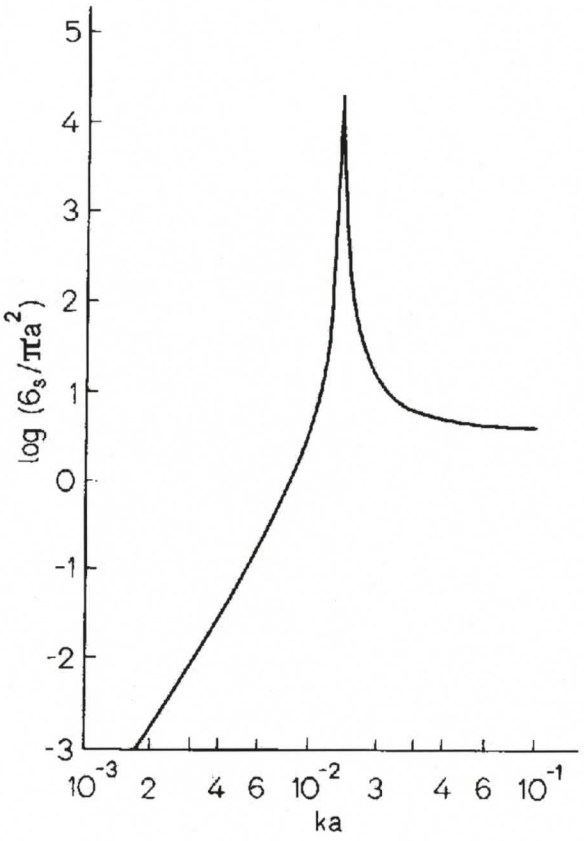

Figure 2.1 Dependence of scattering cross section of an air bubble in water on ka (Only losses due to radiation are taken into account)

At resonance, the total scattering cross section is

$$\sigma_S(f) = \frac{4\pi a^2}{(k_0 a)^2} = \frac{4\pi}{k_0^2} = \frac{\lambda_0^2}{\pi} \tag{2.14}$$

where $\lambda_0 = 2\pi / k_0$ is the resonance wavelength. The total scattering cross section at resonance becomes $4/(k_0 a)^2$ greater than the geometrical cross section. For example, for a resonance bubble near the water surface, $k_0 a = 0.0136$, and it

follows that the bubble radius is small compared to the sound wavelength. Then we obtain $\sigma_S/(\pi a^2) \approx 2.16 \cdot 10^4$, which means the scattering cross section of a bubble at resonance is more than 20,000 times its geometrical one, as shown in Fig.2.1. Energy losses caused by shear viscosity and thermal conductivity somewhat decrease this value, but scattered intensity due to bubble resonance is still dominant. For this reason, an acoustical scattering experimenter has a very easy task to distinguish a rigid sphere from a resonating bubble of the same size.

Fig.2.1 also shows that the intensity of the scattered field rapidly decreases when the difference between the sound frequency and the resonance frequency increases. This gives the important indication that we can measure bubbles with a narrow radius range using acoustical methods that employ the resonance features of the bubbles.

2.2 Nonlinear Scattering by Gas Bubbles in Sediments

2.2.1 Nonlinear Scattering Mechanism

Zabolotskaya and Soluyan (1972) used the variable of the change of volume instead of change of radius in the Rayleigh equation:

$$V' = \frac{4}{3}\pi R^3 \tag{2.15}$$

$$V' = V_\circ + V \tag{2.16}$$

where $V_\circ$ - bubble equilibrium volume;

V - bubble volume change.

Assuming that

1) volume changes are small compared to the equilibrium bubble volume;

2) the pressure of the incident wave is much smaller than the equilibrium pressure;

3) The surface tension can be neglected because it is not significant for bubbles with radius greater than $10\,\mu m$,

Zabolotskaya and Soluyan (1972) derived the equation which describes the changes of bubble volume:

$$\ddot{V} + \omega\delta\dot{V} + \omega_\circ^2 V + \in P = \alpha V^2 + \mu(2\ddot{V}V + \dot{V}^2) \tag{2.17}$$

where ω - the frequency of volume oscillation;

δ - resonant attenuation constant;

$\omega_\circ$ - bubble resonant frequency;

P - acoustic pressure incident upon the bubbles.

Bubble resonant frequency $\omega_\circ$ and coefficients α, μ, $\in$ are defined as follows:

$$\omega_\circ^2 = \frac{3\gamma p_\circ}{\rho_\circ a_\circ^2} \tag{2.18}$$

$$\mu = \frac{1}{8\pi a_\circ^3},\ \alpha = 3\beta(\gamma+1)\omega_\circ^2,\ \in = 4\pi a_\circ / \rho_0 \tag{2.19}$$

where γ - ratio of specific heats of the gas inside the bubble;

p_0 - ambient static pressure;

ρ_0 - ambient medium density;

a_0 - bubble equilibrium radius;

β - thermal conductivity factor.

Eq. (2-17) can be distinguished by the linear part, which is on the left side of the equation, and the two nonlinear parts, which are on the right side of the equation. αV^2 is the consequence of adiabatic behavior of gas inside the bubble, and $\mu(2\ddot{V}V + \dot{V}^2)$ is the dynamic nonlinearity.

For bubbles in water, sound attenuation and velocity are not dependent on frequency. But for bubbles in sediment, the non-homogeneous medium, they both depend on frequency.

The quantities $\omega_\circ$, α, δ, and $\in$ will vary with the applied frequency since they depend on the fluid density ρ_0, which effectively varies with frequency in the context of the Biot Theory (Boyle and Chotiros 1998). This indicates that the gas bubble does not possess a unique resonance frequency, instead its resonance frequency varies with the applied frequency.

But for simplification, we assume a special case that the gas bubble is surrounded by a simple medium, where ω_0, α and δ are all independent of frequency (Zabolotskaya and Soluyan 1973).

Consider two acoustic waves incident upon the bubble:

$$P = P_1 \cos(\omega_1 t + \varphi_1) + P_2 \cos(\omega_2 t + \varphi_2) \tag{2.20}$$

where P_1 and P_2 are the amplitudes, and φ_1 and φ_2 are corresponding phases of the two superimposed incident acoustic waves with frequencies of ω_1 and ω_2 respectively.

For gas bubble in the field of two plane and sinusoidal waves, Eq. (2.17) can be written as:

$$\ddot{V} + \omega\delta\dot{V} + \omega_\circ^2 V = -\in [P_1 \cos(\omega_1 t + \varphi_1) + P_2 \cos(\omega_2 t + \varphi_2)] + \alpha V^2 + \mu(2\ddot{V}V + \dot{V}^2). \tag{2.21}$$

Let V be of the form

$$V = \sum_{n=0} o^n V^{(n)} \tag{2.22}$$

where $o << 1$.

Substitute (2.22) into (2.21), and compare expressions with corresponding powers, we can obtain the following two equations:

$$\ddot{V}^{(0)} + \omega\delta\dot{V}^{(0)} + \omega_{\circ}^{2}V^{(0)} = -\in[P_1\cos(\omega_1 t + \varphi_1) + P_2\cos(\omega_2 t + \varphi_2)] \tag{2.23}$$

$$\ddot{V}^{(1)} + \omega\delta\dot{V}^{(1)} + \omega_{\circ}^{2}V^{(1)} = \alpha V^{(0)^2} + \mu(2\ddot{V}^{(0)}V^{(0)} + \dot{V}^{(0)^2}). \tag{2.24}$$

The solution of Eq. (2.23) gives the amplitudes of the volume changes for linear components V_{ω_1} and V_{ω_2}

$$V_{\omega_1} = \frac{\in P_1}{\sqrt{\left(\omega_0^2 - \omega_1^2\right)^2 + \delta^2\omega_1^4}} \tag{2.25}$$

$$V_{\omega_2} = \frac{\in P_2}{\sqrt{\left(\omega_0^2 - \omega_2^2\right)^2 + \delta^2\omega_2^4}} \tag{2.26}$$

To obtain the results for nonlinear components, substitute Eq. (2.25) and Eq. (2.26) into Eq. (2.24), then we obtain the amplitudes of volume changes for double, sum and different frequencies:

$$V_{2\omega_1} = \frac{\in^2\left(\alpha - 3\mu\omega_1^2\right)P_1^2}{2\left[\left(\omega_0^2 - \omega_1^2\right)^2 + \delta^2\omega_1^4\right]\sqrt{\left(\omega_0^2 - 4\omega_1^2\right)^2 + 16\delta^2\omega_1^4}} \tag{2.27}$$

$$V_{2\omega_2} = \frac{\in^2\left(\alpha - 3\mu\omega_2^2\right)P_2^2}{2\left[\left(\omega_0^2 - \omega_2^2\right)^2 + \delta^2\omega_2^4\right]\sqrt{\left(\omega_0^2 - 4\omega_2^2\right)^2 + 16\delta^2\omega_2^4}} \tag{2.28}$$

$$V_{\Omega_+} = \frac{\in^2[\alpha - \mu(\omega_1^2 + \omega_2^2 + \omega_1\omega_2)]P_1P_2}{\sqrt{\left(\omega_0^2 - \omega_1^2\right)^2 + \delta^2\omega_1^4}\sqrt{\left(\omega_0^2 - \omega_2^2\right)^2 + \delta^2\omega_2^4}\sqrt{\left(\omega_0^2 - \Omega_+^2\right)^2 + \delta^2\Omega_+^4}} \tag{2.29}$$

$$V_{\Omega_-} = \frac{\in^2[\alpha - \mu(\omega_1^2 + \omega_2^2 - \omega_1\omega_2)]P_1P_2}{\sqrt{\left(\omega_0^2 - \omega_1^2\right)^2 + \delta^2\omega_1^4}\sqrt{\left(\omega_0^2 - \omega_2^2\right)^2 + \delta^2\omega_2^4}\sqrt{\left(\omega_0^2 - \Omega_-^2\right)^2 + \delta^2\Omega_-^4}} \tag{2.30}$$

where $\Omega_+ = \omega_1 + \omega_2$, $\Omega_- = \omega_1 - \omega_2$. The subscripts 1, 2, Ω_+, and Ω_- represents the acoustic oscillating frequency of the gas bubble.

When the bubble volume is oscillating with frequencies of ω_1, ω_2, $2\omega_1$, $2\omega_2$, Ω_-, and Ω_-, the compressional waves will be generated in a distance of r from

the center of the bubble in the surrounding medium. The relation between the far-field acoustic pressure amplitude P_{ω_i} and the volume perturbation amplitude V_{ω_i} is given by (Zabolotskaya and Soluyan 1973)

$$P_{\omega_i} = \frac{\omega_i^2 \rho_0 V_{\omega_i}}{4\pi r}. \tag{2.31}$$

Upon substituting Eq. (2.25)- Eq. (2.30) for V_{ω_i} in Eq. (2.31), we obtain the pressure amplitudes for linear components

$$P_{\omega_1} = \frac{\omega_1^2 a_\circ P_1}{\sqrt{\left(\omega_0^2 - \omega_1^2\right)^2 + \delta^2 \omega_1^4}} \cdot \frac{1}{r} \tag{2.32}$$

$$P_{\omega_2} = \frac{\omega_2^2 a_\circ P_2}{\sqrt{\left(\omega_0^2 - \omega_2^2\right)^2 + \delta^2 \omega_2^4}} \cdot \frac{1}{r} \tag{2.33}$$

and the pressure amplitudes for nonlinear components

$$P_{2\omega_1} = \frac{3\omega_1^2 \left((\gamma+1)\omega_0^2 - \omega_1^2\right) P_1^2}{\rho_\circ a_\circ \left[\left(\omega_0^2 - \omega_1^2\right)^2 + \delta^2 \omega_1^4\right] \sqrt{\left(\omega_0^2 - 4\omega_1^2\right)^2 + 16\delta^2 \omega_1^4}} \cdot \frac{1}{r} \tag{2.34}$$

$$P_{2\omega_2} = \frac{3\omega_2^2 \left((\gamma+1)\omega_0^2 - \omega_2^2\right) P_2^2}{\rho_\circ a_\circ \left[\left(\omega_0^2 - \omega_2^2\right)^2 + \delta^2 \omega_2^4\right] \sqrt{\left(\omega_0^2 - 4\omega_2^2\right)^2 + 16\delta^2 \omega_2^4}} \cdot \frac{1}{r} \tag{2.35}$$

$$P_{\Omega_+} = \frac{\Omega_+^2 [3(\gamma+1)\omega_0^2 - \left(\omega_1^2 + \omega_2^2 + \omega_1\omega_2\right)] P_1 P_2}{2\rho_\circ a_\circ \sqrt{\left(\omega_0^2 - \omega_1^2\right)^2 + \delta^2 \omega_1^4} \sqrt{\left(\omega_0^2 - \omega_2^2\right)^2 + \delta^2 \omega_2^4} \sqrt{\left(\omega_0^2 - \Omega_+^2\right)^2 + \delta^2 \Omega_+^4}} \cdot \frac{1}{r} \tag{2.36}$$

$$P_{\Omega_-} = \frac{\Omega^2 [3(\gamma+1)\omega_\circ^2 - \mu\left(\omega_1^2 + \omega_2^2 - \omega_1\omega_2\right)] P_1 P_2}{2\rho_\circ a_\circ \sqrt{\left(\omega_0^2 - \omega_1^2\right)^2 + \delta^2 \omega_1^4} \sqrt{\left(\omega_0^2 - \omega_2^2\right)^2 + \delta^2 \omega_2^4} \sqrt{\left(\omega_0^2 - \Omega_-^2\right)^2 + \delta^2 \Omega_-^4}} \cdot \frac{1}{r} \tag{2.37}$$

Thus as a result of the interaction of two sinusoidal waves with a gas bubble, acoustic waves are emitted with frequencies ω_1, ω_2, $2\omega_1$, $2\omega_2$, Ω_-, and Ω_-, whose amplitudes are described by Eq. (2.32)-Eq. (2.37) above.

2.2.2 Scattering Cross Sections

As mentioned earlier in this chapter, the scattering cross section is the ratio of the power radiated by scattering element to the intensity of incident wave. In the GABI project, the cross sections of the primary, sum, difference and double frequencies of the pulsating bubble are studied.

We can rewrite Eq. (2.8) as

$$\sigma = 4\pi r^2 \left| \frac{P_S}{P_i} \right|^2 \tag{2.38}$$

where P_S is the pressure of the scattered wave at a specific frequency, and P_i is the pressure of the incident wave.

Based on Eq. (2.32)-Eq. (2.37) which give the expression for the pressure of the scattered waves at different frequencies, the scattering cross sections of bubbles embedded in soft water-saturated sediments for different components could be estimated using Eq. (2.38) as follows:

$$\sigma_{\omega_1} = \frac{4\pi a_\circ^2 \omega_1^4}{\left[\left(\omega_\circ^2 - \omega_1^2\right)^2 + \delta^2 \omega_1^4\right]} \tag{2.39}$$

$$\sigma_{\omega_2} = \frac{4\pi a_\circ^2 \omega_2^4}{\left[\left(\omega_\circ^2 - \omega_2^2\right)^2 + \delta^2 \omega_2^4\right]} \tag{2.40}$$

$$\sigma_{2\omega_1} = \frac{36\pi\omega_1^4 \left[(\gamma+1)\omega_\circ^2 - \omega_1^2\right]^2 P_1^2}{\rho_\circ^2 a_\circ^2 \left[\left(\omega_\circ^2 - \omega_1^2\right)^2 + \delta^2 \omega_1^4\right]^2 \left[\left(\omega_\circ^2 - 4\omega_1^2\right)^2 + 16\delta^2 \omega_1^4\right]} \tag{2.41}$$

$$\sigma_{2\omega_2} = \frac{36\pi\omega_2^4 \left[(\gamma+1)\omega_\circ^2 - \omega_2^2\right]^2 P_2^2}{\rho_\circ^2 a_\circ^2 \left[\left(\omega_\circ^2 - \omega_2^2\right)^2 + \delta^2 \omega_2^4\right]^2 \left[\left(\omega_\circ^2 - 4\omega_2^2\right)^2 + 16\delta^2 \omega_2^4\right]} \tag{2.42}$$

$$\sigma_{\Omega_-} = \frac{\pi\Omega_-^4 \left[3(\gamma+1)\omega_\circ^2 - \left(\omega_1^2 + \omega_2^2 - \omega_1\omega_2\right)\right]^2 P_1 P_2}{\rho_\circ^2 a_\circ^2 \left[\left(\omega_\circ^2 - \omega_1^2\right)^2 + \delta^2 \omega_1^4\right]\left[\left(\omega_\circ^2 - \omega_2^2\right)^2 + \delta^2 \omega_2^4\right]\left[\left(\omega_\circ^2 - \Omega_-^2\right)^2 + \delta^2 \Omega_-^4\right]} \tag{2.43}$$

$$\sigma_{\Omega_+} = \frac{\pi\Omega_+^4\left[3(\gamma+1)\omega_\circ^2 - \left(\omega_1^2+\omega_2^2+\omega_1\omega_2\right)\right]^2 P_1P_2}{\rho_\circ^2 a_\circ^2\left[\left(\omega_\circ^2-\omega_1^2\right)^2+\delta^2\omega_1^4\right]\left[\left(\omega_\circ^2-\omega_2^2\right)^2+\delta^2\omega_2^4\right]\left[\left(\omega_\circ^2-\Omega_+^2\right)^2+\delta^2\Omega_+^4\right]} \quad (2.44)$$

It is obvious that the scattering cross section for nonlinear components $\{2\omega_{1,2}$, $\omega_1+\omega_2, \omega_1-\omega_2\}$ are dependent on the incident waves pressure P_1 and P_2, which is different from the linear case described in Eq. (2.39) and Eq. (2.40).

These Eq. (2.39)-Eq. (2.44) describe the scattering features only for a single bubble. As for a distribution of bubbles, the total scattering cross section of the unit volume is approximately equal to the sum of cross sections for each bubble, assuming that there is no interaction between bubbles.

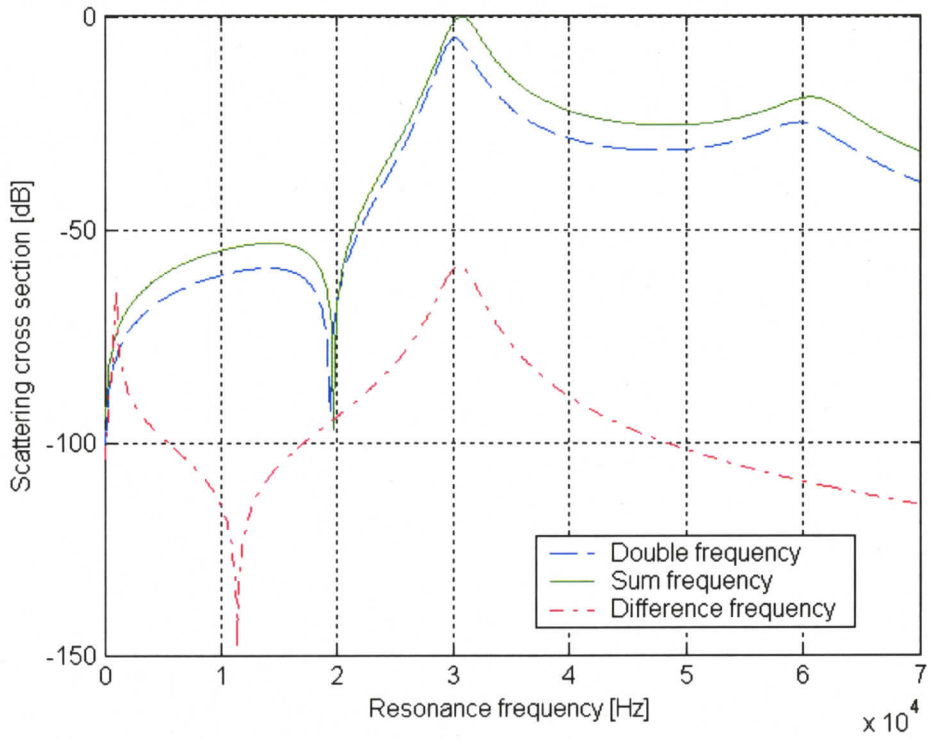

Figure 2.2 Scattering cross section for the double, sum and difference frequency components (normalized by the maximum value of scattering cross section at sum frequency) as a function of bubble resonance frequency, where the incident frequencies are chosen at 30 kHz and 31 kHz.

If there is a single incident wave upon the bubble, the bubble will oscillate at primary, double, and possibly higher harmonic frequencies. But for a nonlinear method with two incident waves upon the bubble, the characteristic frequencies that the bubble oscillation will generate are the sum and difference frequency. So theoretically the difference and sum frequency components will give the most selective feature for gas bubble identification.

In order to compare the features of the scattering cross section at double, sum and difference frequencies, Fig.2.2 gives the plot, based on Eq. (2.42)-Eq. (2.44), of the scattering cross section as a function of bubble resonance frequency when the incident waves are at 30 kHz & 31 kHz. Fig.2.2 shows some important facts for the scattering cross section.

Firstly, for the cross section of double frequency component, there are two maximums when $\omega_0 = \omega_1$ and $\omega_0 = 2\omega_1$. For the cross section of sum frequency component, three maximums happen when $\omega_0 = \omega_1$, $\omega_0 = \omega_2$, and $\omega_0 = \omega_1 + \omega_2$. As to the cross section of difference frequency component, there are also three maximums when $\omega_0 = \omega_1$, $\omega_0 = \omega_2$, and $\omega_0 = |\omega_1 - \omega_2|$. This can be explained if we take a look on the denominators of Eq. (2.42)-Eq. (2.44). The scattering crosss section will reach maximum when any item of the denominators equals to zero.

Secondly, since the transmitting frequencies are chosen at $\omega_1 = 30$ kHz and $\omega_2 = 31$ kHz, which are very close to each other, the maximum cross section for both the sum and difference frequency components at $\omega_0 = \omega_1$ and $\omega_0 = \omega_2$ are overlapping. But if we choose a bigger interval between ω_1 and ω_2, the two maximums of the cross section for sum and difference frequency component at $\omega_0 = \omega_1$ and $\omega_0 = \omega_2$ will be resolved.

Thirdly, the scattering cross section of difference frequency component is much smaller than that of the sum frequency component at the two maximums when bubble resonance frequency is equal to the incident wave frequencies. This indicates that the sum frequency component should be more useful for bubble identification, since the strength of backscattered signal at the sum frequency would be much greater than the backscattered signal at the difference frequency if we are considering the backscattering from a distribution of bubbles.

Fourthly, among the three maximum cross section values of the difference frequency component, the one at $\omega_0 = |\omega_1 - \omega_2| = 1$ kHz is smaller than the other two maximums at $\omega_0 = 30$ kHz and $\omega_0 = 31$ kHz. Similarly, for sum frequency component, the maximum cross section values at $\omega_0 = 30$ kHz and $\omega_0 = 31$ kHz are bigger than the one when $\omega_0 = \omega_1 + \omega_2 = 61$ kHz. From this fact we can have an important inference that the backscattered signal at nonlinear frequencies Ω_- and Ω_+ are mainly contributed by the gas bubbles that are resonating at primary frequencies ω_1 and ω_2.

Fifthly, when the interval between ω_1 and ω_2 is approaching zero, the cross section of sum frequency component is four times that of the double frequency component $\sigma_{\Omega_+} = 4\sigma_{2\omega_1}$. We can deduct this result by assuming $\omega_1 = \omega_2$, and substitue $2\omega_1$ for Ω_+ in Eq. (2.44). Since the interval between ω_1 and ω_2 is 1 kHz for Fig.2.2, we can see from this figure that $\sigma_{2\omega_1}$ is slightly smaller than σ_{Ω_+} when $\omega_0 = \omega_1$. If we increase the primary frequency interval, then $\sigma_{2\omega_1}$ will keep increasing and even exceed σ_{Ω_+}.

The last noticable fact in Fig. 2.2 is that each scattering cross section has a minimum. This is due to the fact that the numerators in Eq. (2.42)-Eq. (2.44) can

be zero. For example, in Eq. (2.42), when $(\gamma+1)\omega_\circ^2-\omega_1^2=0$, $\sigma_{2\omega_1}$ reaches zero where ω_0 is about 20kHz; in Eq.(2.43), $3(\gamma+1)\omega_\circ^2-\left(\omega_1^2+\omega_2^2-\omega_1\omega_2\right)=0$, σ_{Ω_-} reaches zero where ω_0 is at about 12 kHz.

So far the most important facts we obtain from Eq. (2.42)-Eq. (2.44) and Fig.2.2 are that the sum frequency component will offer the most practical means for bubble measurements, and the backscattered signal at sum frequency is mostly contributed by gas bubbles resonating at trasmitting frequencies. In order to improve the efficiency and reliability of the nonlinear measurement method, we have two means to increase the backscattered signal strength at sum frequency.

One way is to decrease the interval between the primary frequencies. We know that when incident waves frequencies ω_1 and ω_2 are getting closer to each other, the peaks of the scattering cross section will be overlapping, and the shapes of the peaks are becoming narrower and the maximum value increases. For a sufficiently small interval between ω_1 and ω_2, the scattering energy comes almost only from the bubbles resonating at a range between ω_1 and ω_2. This is demonstrated by the results of the computations made for different intervals $\Delta\omega$ between ω_1 and ω_2 (Tegowski 2003).

From Figure2.3 (a-b), we can see that decreasing the interval between ω_1 and ω_2 helps obtain good energy efficiency for the scattering process, especially for sum frequency. As a result, it is necessary to choose close frequencies of the incident waves for nonlinear mesurement of bubbles.

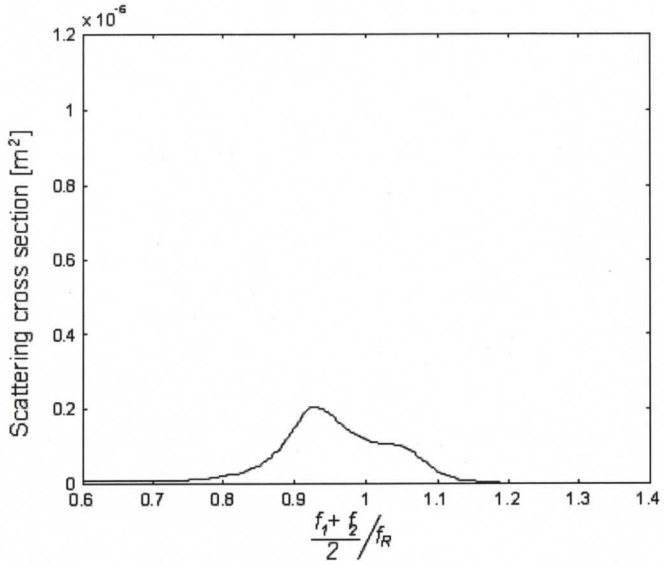

Figure 2.3 (a) Dependence of scattering cross section of sum component on the arithmetical mean of incident frequencies normalized by bubble resonance frequency when $\Delta f = 5\,\mathrm{kHz}$

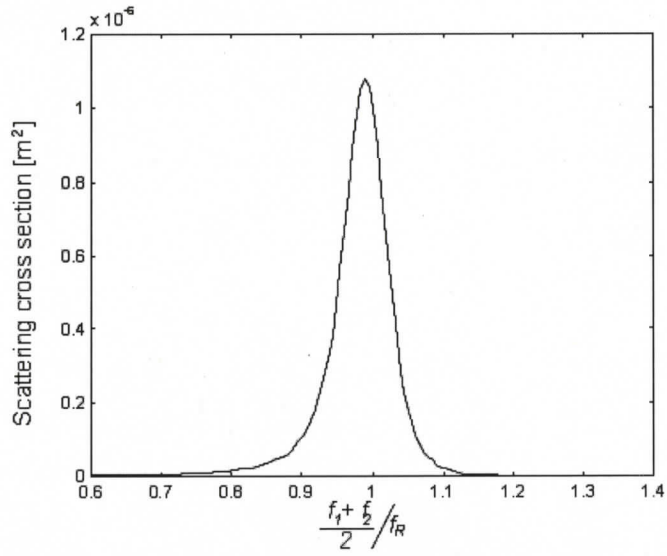

Figure 2.3 (b) Dependence of scattering cross section of sum component on the arithmetical mean of incident frequencies normalized by bubble resonance frequency when $\Delta f = 1\,\mathrm{kHz}$ (Figure courtesy of J. Tegowski)

The other way is to increase the amplitude of the transmitting waves. It is obvious that the scattering cross section for nonlinear components are dependent on incident wave pressure P_1 and P_2. If we need to increase the maximum of nonlinear cross section at resonance, we can also try increasing incident wave pressure. However, we should also take into consideration that incident wave pressure should satisfy the relation: $P_1 / P_0 << 1$ and $P_2 / P_0 << 1$, which is one of the assumptions that Eq. (2.17) describing the bubble volume change is based on.

2.2.3 Volume Scattering Coefficient

Eq. (2.39)-Eq. (2.44) describe the scattering features of a single bubble only. For bubble concentration measurement, we need to derive the sum of the scattering cross sections of the bubble set. We make the following assumptions:

1) The transmitting frequencies are similar, $\omega_1 \approx \omega_2$;
2) The scattered signal mainly comes from bubbles with resonant frequency which is equal to the arithmetical mean of the incident wave frequencies, $\omega_0 = (\omega_1 + \omega_2)/2$;
3) The function of bubbles density in insonified volume is a constant.

The volume scattering coefficient is defined as

$$\beta = \int_0^\infty n(a_0)\sigma(a_0)da_0 \tag{2.45}$$

where a_0 is the equilibrium bubble radius, and $n(a_0)$ is the bubble size density function, which is defined as

$$n(a_0) = dN(a_0)/da_0 \tag{2.46}$$

where $N(a_0)$ is the number of bubbles with radii less than a_0 per unit volume.

According to Eq. (2.44), the volume scattering coefficient for sum frequency can be written as:

$$\beta_{\Omega_+} = \int_0^{\infty} \frac{\pi\Omega_+^4\left[3(\gamma+1)\omega_\circ^2 - \left(\omega_1^2+\omega_2^2+\omega_1\omega_2\right)\right]^2 P_1P_2}{\rho_\circ^2 a_\circ^2\left[\left(\omega_\circ^2-\omega_1^2\right)^2+\delta^2\omega_1^4\right]\left[\left(\omega_\circ^2-\omega_2^2\right)^2+\delta^2\omega_2^4\right]\left[\left(\omega_\circ^2-\Omega_+^2\right)^2+\delta^2\Omega_+^4\right]} \times n(a_\circ)da_\circ$$

$$= \frac{\pi\Omega_+^4\left[3(\gamma+1)\omega_\circ^2 - \left(\omega_1^2+\omega_2^2+\omega_1\omega_2\right)\right]^2 P_1P_2}{\rho_\circ^2\left[\left(\omega_\circ^2-\Omega_+^2\right)^2+\delta^2\Omega_+^4\right]\omega_1^4\omega_2^4} \times n(a_r)\times$$

$$\int_{a_r-\Delta a_r}^{a_r+\Delta a_r} \frac{da_\circ}{a_\circ^2\left[\left(\frac{\omega_\circ^2}{\omega_1^2}-1\right)^2+\delta^2\right]\left[\left(\frac{\omega_\circ^2}{\omega_2^2}-1\right)^2+\delta^2\right]} \tag{2.47}$$

where a_r is the radius of bubbles at resonance. The integration is over $2\Delta a_r$ which is the half width of the peak of the scattering cross section near primary frequencies.

Based on Eq.(2.18), which describes the relationship between the resonant frequency and radius of the gas bubble, if a bubble with equilibrium radius a_0 has a resonant frequency of ω_0, the bubble with radius a_r can be related in the same way with resonant frequency ω, then we can write:

$$\frac{\omega_0^2}{\omega^2} = \frac{a_r^2}{a_0^2} \tag{2.48}$$

If there is small difference between transmitting frequencies, the integral part of Eq. (2.47) can be written as:

$$I = \int_{a_r-\Delta a_r}^{a_r+\Delta a_r} \frac{da_\circ}{a_\circ^2\left[\left(\frac{a_r^2}{a_\circ^2}-1\right)^2+\delta^2\right]^2} \tag{2.49}$$

After the substitution

$$q = \frac{a_r}{a_\circ} - 1, \quad dq = -\frac{a_r}{a_\circ^2}da_\circ \tag{2.50}$$

and the approximation

$$(q(q+2))^2 = q^4 + 4q^3 + 4q^2 \approx 4q^2 \qquad q << 1, \tag{2.51}$$

the integral can be written as

$$I = -\int_{q_1}^{q_2} \frac{dq}{a_r\left[(q(q+2))^2 + \delta^2\right]^2} \approx -\int_{q_1}^{q_2} \frac{dq}{a_r\left[4q^2 + \delta^2\right]^2} = \frac{1}{a_r}\int_{-\infty}^{+\infty} \frac{dq}{\left[4q^2 + \delta^2\right]^2} = \frac{\pi}{4a_r\delta^3} \tag{2.52}$$

where $q_1 = \dfrac{a_r}{a_r - \Delta a_r} - 1$, $q_2 = \dfrac{a_r}{a_r + \Delta a_r} - 1$. The limits of integration have been expanded to infinity since the contribution to the integral is small outside the original limits of q_1 and q_2.

Using the calculation result of the integral in Eq. (2.52), we can obtain the expression for volume scattering coefficient at sum frequency:

$$\beta_{\Omega_+} = \frac{\pi\Omega_+^4\left[3(\gamma+1)\omega_\circ^2 - \left(\omega_1^2 + \omega_2^2 + \omega_1\omega_2\right)\right]^2 P_1P_2}{\rho_\circ^2\left[\left(\omega_\circ^2 - \Omega_+^2\right)^2 + \delta^2\Omega_+^4\right]\omega_1^4\omega_2^4} \times n(a_r) \times \frac{\pi}{4\delta^3 a_r}. \tag{2.53}$$

In the same way, the expressions for volume scattering coefficients at the double and difference frequencies are obtained:

$$\beta_{2\omega_{1,2}} = \frac{36\pi\left[(\gamma+1)\omega_\circ^2 - \omega_{1,2}^2\right]^2 P_1P_2}{\rho_\circ^2\left[\left(\omega_\circ^2 - 4\omega_{1,2}^2\right)^2 + 16\delta^2\omega_{1,2}^4\right]\omega_{1,2}^4} \times n(a_r) \times \frac{\pi}{4\delta^3 a_r} \tag{2.54}$$

$$\beta_{\Omega_-} = \frac{\pi\Omega_+^4\left[3(\gamma+1)\omega_\circ^2 - \left(\omega_1^2 + \omega_2^2 - \omega_1\omega_2\right)\right]^2 P_1P_2}{\rho_\circ^2\left[\left(\omega_\circ^2 - \Omega_-^2\right)^2 + \delta^2\Omega_-^4\right]\omega_1^4\omega_2^4} \times n(a_r) \times \frac{\pi}{4\delta^3 a_r}. \tag{2.55}$$

2.3 Inversion for bubble concentration

Based on the nonlinear scattering mechanisms of gas bubbles described in the previous section, the inversion process of bubble backscattering data for bubble concentration involves the calculation of scattering volume, which is the

common area of the two transmitting beams, and the theoretical model of bubble concentration inversion.

2.3.1 Scattering Volume

In this section, the geometrical scattering volume will be discussed in the setting of the nonlinear measurement method for the inversion of bubble density. The scattering volume will be estimated numerically for different transducer configurations based on predicted beam patterns and their common part.

For the two plane waves propagating in the same direction, the field intensity in the point where both pulses arrive is equal to the half of the sum of the two wave intensities. Linear dependency of wave intensity on the squared acoustical pressures at a distance of 1m from each of the transmitters allows for the use of the following approximation:

$$I_1 + I_2 \approx P_1^2 + P_2^2 = P_1 P_2 \left(\frac{P_1}{P_2} + \frac{P_2}{P_1}\right) \approx 2 P_1 P_2 \tag{2.56}$$

The acoustical field generated by the circular piston transducers has the axial symmetry. For a single transducer the directivity function in the far field depends on elevation angle only (Clay and Medwin 1977; Urick 1975):

$$b(\theta) = \frac{2J_1(ka\sin\theta)}{ka\sin\theta} \tag{2.57}$$

where: J_1 - Bessel function of the first kind and the first order;

k - acoustical wave number;

a - radius of circular transducer;

θ - angle between the examined direction and the acoustical axis of the transducer.

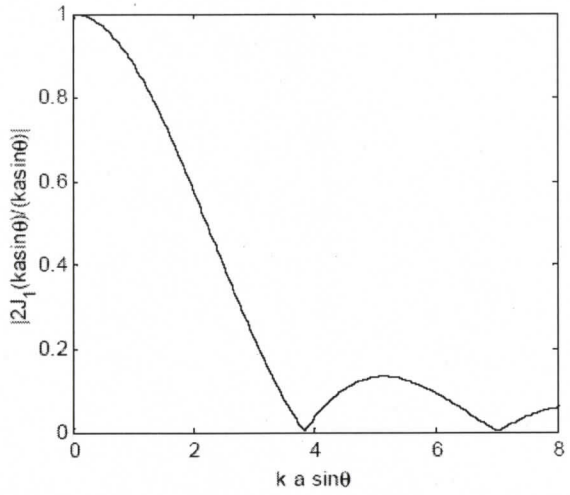

Figure 2.4 Directivity function of a circular transducer

For a transmitting system composed of two transducers, the directivity function is proportional to the product of the directivity functions of the two transducers. The intensity of the acoustical field at the point $P(r_0, \Theta_0, \varphi_0)$ for the far zone ($r > \pi D^2 / 4\lambda$) can be described as follows:

$$I_0(r,\Theta,\varphi) = \frac{P_1 \cdot b_1(\Theta_1)}{r_1} \cdot \frac{P_2 \cdot b_2(\Theta_2)}{r_2}$$

$$= \frac{P_1}{r_1} \cdot \frac{2J_1(k_1 a_1 \sin\Theta_1)}{k_1 a_1 \sin\Theta_1} \times \frac{P_2}{r_2} \cdot \frac{2J_2(k_2 a_2 \sin\Theta_2)}{k_2 a_2 \sin\Theta_2} \qquad (2.58)$$

where Θ_i is the angle between the acoustical axis and the radius r_i of the i-th transducer, as shown in Fig.2.5.

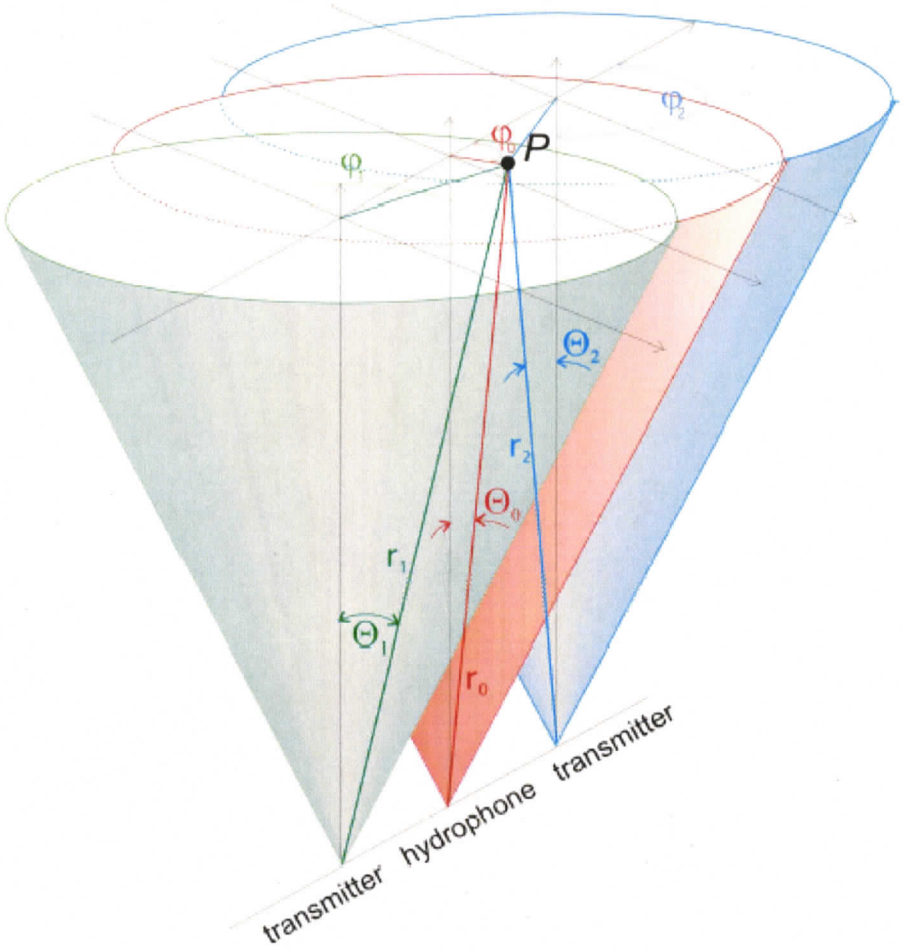

Figure 2.5 Geometry of transmitting-receiving system
(Figure courtesy of J. Tegowski)

If the transmitting pulse width is τ, the sound speed in the transmitting medium is c, then the scattering volume at time t is defined as the common part of the spherical layer, which has a thickness of $d = c\tau/2$ at a distance of $r = ct/2$ from the receiver, and the directivity function of the transmitting system. Since the axes of the transmitters and the hydrophone are parallel, as Fig.2.5 shows, the computations of scattering volume were made using the following algorithm:

1) The center of the coordinate system was placed in the center of the hydrophone at point (0,0,0) . The distance from the beginning of the coordinate system to the point on the axis y was divided by s elements separated one from another by $r_s = ct_s / 2$, where $s = 1,2,...N$, and t_s is the array of numbers from which the consecutive signal samples was taken. For each chosen distance r_s, it was assigned a plane perpendicular to the transmitters and receiver axes.
2) Each of the cutting planes is associated with local Cartesian coordinate system OXY with the center in cross point of the plane and the hydrophone acoustical axis. The next step is to construct a net with mΔx in X axis and nΔy in Y axis, m,n=0,±1,±2,..., Δx=Δy.
3) For each cell of the net in the cutting plane that is at a distance $r = ct/2$ from the receiver, the product of directivity functions of the receiving-transmitting system is computed as:

$$\Psi_{mn}(r_{mn},\Theta_{mn},\varphi_{mn}) = \frac{1}{r_{1mn}} \cdot \frac{2J_1(k_1 a_1 \sin(\Theta_{1mn})}{k_1 a_1 \sin(\Theta_{1mn})} \times \times \frac{1}{r_{2mn}} \cdot \frac{2J_1(k_2 a_2 \sin(\Theta_{2mn})}{k_2 a_2 \sin(\Theta_{2mn})} \times \frac{1}{r_{0mn}} \frac{2J_1(k_0 d_0 \sin(\Theta_{0mn})}{k_0 d_0 \sin(\Theta_{0mn})} \tag{2-59}$$

and multiplied by the cell area ΔxΔy.

The result of this algorithm is the cross part of the directivity functions of the receiving-transmitting system. Fig.2.6 shows an example of the cross part of the directivity function of the receiving-transmitting system. The cross area is perpendicular to the acoustical axis of hydrophone, at a distance of 10m

from the hydrophone, and the transmitted frequencies are 30.4 kHz and 33.6 kHz.

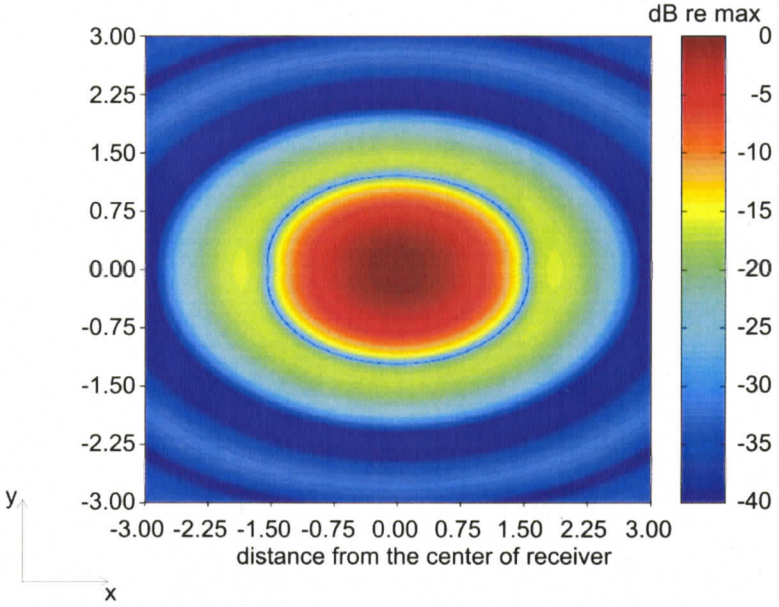

Figure 2.6 Example of cross area of transmitting-receiving system for a cutting plane 10m from the transmitter (transmitting frequencies at 30.2 kHz & 33.4 kHz)

Each element of the cross part has a color, which corresponds to its weight. Values of weights are taken to computations of scattering volume. Only those points $S_{mn} = \Psi_{mn} \times \Delta x \times \Delta y$ with value equal or bigger than –3 dB were taken into consideration.

$$S_0(r_s) = \left\{ S_{mn}(r_s), \quad 10\log_{10}\frac{S_{mn}(r_s)}{\max(S_{mn}(r_s))} \geq -3\ dB \right\} \tag{2.60}$$

The equivalent scattering volume can be calculated by integrating the function $S_0(r_s)$ using to the following equation:

$$V(r_s) = \int_{r_s}^{r_s+\frac{c\tau}{2}} S_0(r_s)\,dr_s \tag{2.61}$$

The scattering volume is a function of the distance from the hydrophone.

Fig.2.7 shows the dependence of equivalent scattering volume at different frequencies on the distance from the hydrophone.

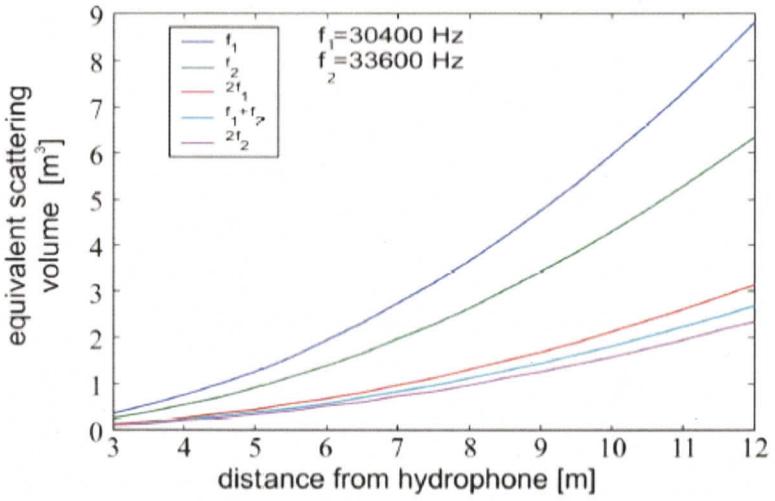

Figure 2.7 The dependence of equivalent scattering volume on the distance from the hydrophone

2.3.2 Bubble Concentration Inversion

The physical model that describes the nonlinear scattering process is the basis for the inversion of bubble backscattering data for bubble concentration. This model for the nonlinear method in the GABI project is represented by the echosounder equation, which determines each of the linear as well as nonlinear components:

$$\frac{I_{SC}\{\omega,2\omega,\omega_1-\omega_2,\omega_1+\omega_2\}}{I_0}=\frac{\beta\{\omega,2\omega,\omega_1-\omega_2,\omega_1+\omega_2\}\Delta V\{\omega,2\omega,\omega_1-\omega_2,\omega_1+\omega_2\}}{4\pi r^4} \tag{2.62}$$

where

I_{SC} - backscattered sound intensity for each linear and nonlinear component;

I_0 - sound intensity of the incident waves;

ΔV - scattering volume, different at linear and nonlinear frequencies, and is estimated numerically for different transducer configurations from predicted beam patterns and their common part;

$\beta\{\omega, 2\omega, \omega_1 - \omega_2, \omega_1 + \omega_2\}$ - volume backscattering coefficients for different backscattering processes;

r - distance from the receiver to the scattering processes;

ω_1, ω_2 - transmitting frequencies.

We can calculate the left part of the equation by computing the ratio of backscattered signal strength from the data obtained to the transmitting signal strength; the distance r can be easily determined by the time delay of the echo signal; the scattering volume ΔV can be calculated using the algorithm described in the previous section. From these known values, we can calculate the volume backscattering coefficient $\beta\{\omega, 2\omega, \omega_1 - \omega_2, \omega_1 + \omega_2\}$ based on Eq. (2.62). With the calculation results of scattering cross section at different frequency components $\sigma\{\omega, 2\omega, \omega_1 - \omega_2, \omega_1 + \omega_2\}$, we can conduct the inversion process based on Eq. (2.53)-(2.55) for the bubble concentration $n(a)da$, which is the number of bubbles of radius between a and $a + da$ per unit volume.

Chapter 3

Experimental Setup

Based on the nonlinear scattering theory for gas bubbles in the sediments, the experiments employing nonlinear acoustic methods were carried out in a shallow water area, about 30 meters depth, of the southern part of the Baltic Sea, on board two Polish research vessels, "Oceania" and "Dr.Lubecki".

3.1 Hardware Description

The measurements of the nonlinear scattering of acoustical waves of gas bubbles trapped in the upper layer of sediments were performed as Fig.3.1.

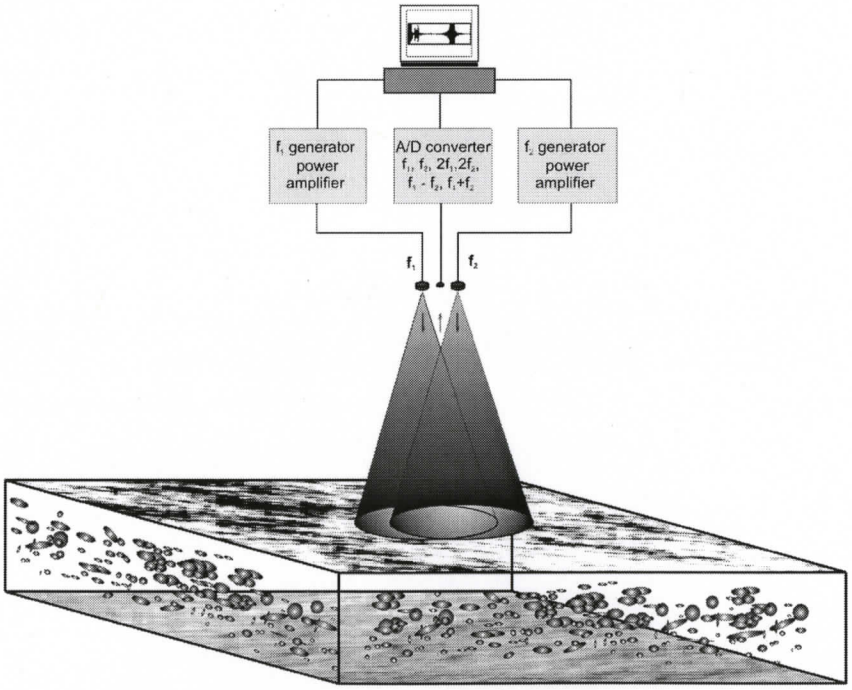

Figure 3.1 Experimental setup scheme of nonlinear measurement system
(Figure courtesy of J. Tegowski)

The experimental system used two transducers to transmit acoustic waves to the surface layer of the sediments. The system was lowered from the ship board on a crane to approximately 10-30 meters above the bottom, with the acoustic beams looking down. The gas bubbles in the surficial layer of the sediment were insonified simultaneously by the two acoustic waves at close frequencies f_1 and f_2. The echo signals from the sea bottom were received at the hydrophone, which was located in the middle of the two transducers. The echo signals were amplified, and digitized with 16-bit resolution for further processing.

A detailed block scheme of the measurement system is shown in Fig.3.2.

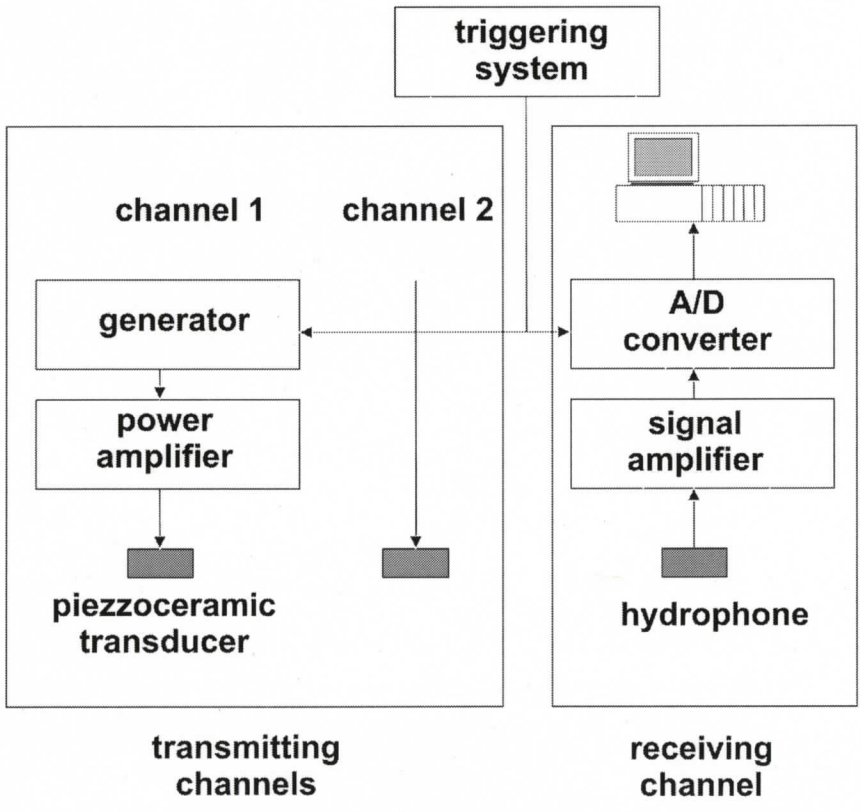

Figure 3.2 Scheme of transmitting-receiving system for nonlinear methods of gas bubbles concentration measurement (Figure courtesy of J. Tegowski)

The transmitting part consisted of two independent channels. Each channel contained a sinusoidal signal generator, a power amplifier and a piezoceramic resonant transducer. The signal generator will generate sinusoidal pulse signals with rectangular envelopes. As a source of power, a two-channel amplifier was used. It was characterized by the low emission of signal harmonic components (the square amplitude of nonlinear component was less than 0.5% of square amplitude of the primary component). The maximal output power of each channel was approximately 1 kW, which was sufficient to form and register the nonlinear effects in the top layer of the sediments where gas bubbles are trapped. During the experiments the average distance between the transducers and the bottom surface was about 25 meters. The power amplifier provided four levels of amplification with output rms voltage of 110V, 240V, 255V, and 270V.

The receiving channel contained a multi-element piston hydrophone, a signal amplifier and an A/D converter. The purpose of locating the receiving signal amplifier so close to the hydrophone was to reduce the ship noise. The GAGE CS1602-1M 16-bit A/D converter was employed and placed inside the computer. Echo signals were sampled using this converter with a sampling frequency of 500 kHz, and the digitized data were saved on a computer.

The transmitting and receiving systems were linked together by a triggering system. The equipment was constructed at the Marine Acoustic laboratory of IOPAS.

During the experiments, the hydro acoustical transducers were located in a steel frame as shown in Fig.3.3.

Figure 3.3 Measurement frame with transducer array (view from the bottom)
(Figure courtesy of J. Tegowski)

Specific parameters of the geometry and the size of the transducer array are shown in Fig.3.4.

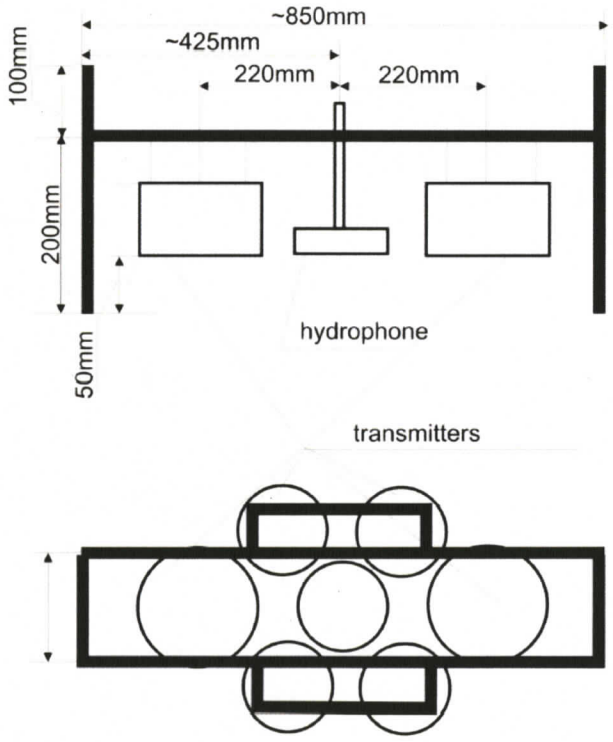

Figure 3.4 Geometry and size of transducers in the measurement system
(Figure courtesy of J. Tegowski)

The diameter of the two transmitters is 0.16 m, while the diameter of the hydrophone is 0.12 m. The closest distance between the edges of the hydrophone and the transmitters is 0.08 m.

The main disadvantage of this measurement system was that it was not capable of making measurements using different pairs of frequencies at the same time or making measurements with small time shift between frequencies, which allow environmental observation in "frozen" state, comparable with time shift between consecutive pulses (Tagowski 2003).

3.2 Area of Investigation

The measurements were performed at selected points distributed in the Gulf of Gdansk area where a geophysical and geological survey was performed earlier and documented. Fig.3.5 displays the geological map of the Baltic Sea bottom developed at the Branch of Marine Geology for the area of the Polish economic zone. The investigated area includes variety of sediments from hard sand mixed with gravel and till to silt and semiliquid organic origin fluffy sediments.

Generally, most shallow water areas of the Gdansk Gulf are covered by marine sands of different grain size, from coarse grained to fine sands. Muddy sediments cover the deeper part of the Gdansk Deep. The thickness of muddy sediments on large area is between 3 and 6 m locally, while reaching a thickness of up to 10m. Water depths at the sampling sites range from 10 to 88 m. Moreover, in the investigated area, there are frequently observed acoustical anomalies, characterised by shallow penetration of acoustical waves into soft sediments. It can be presumed that part of the gases in sediments is the result of

migration out of deeper layers from hydrocarbons deposits (Tegowski *et al.*, 1995).

The map of the sediment type at the Gdansk Gulf is presented in Fig. 3.5, based on the geological survey data.

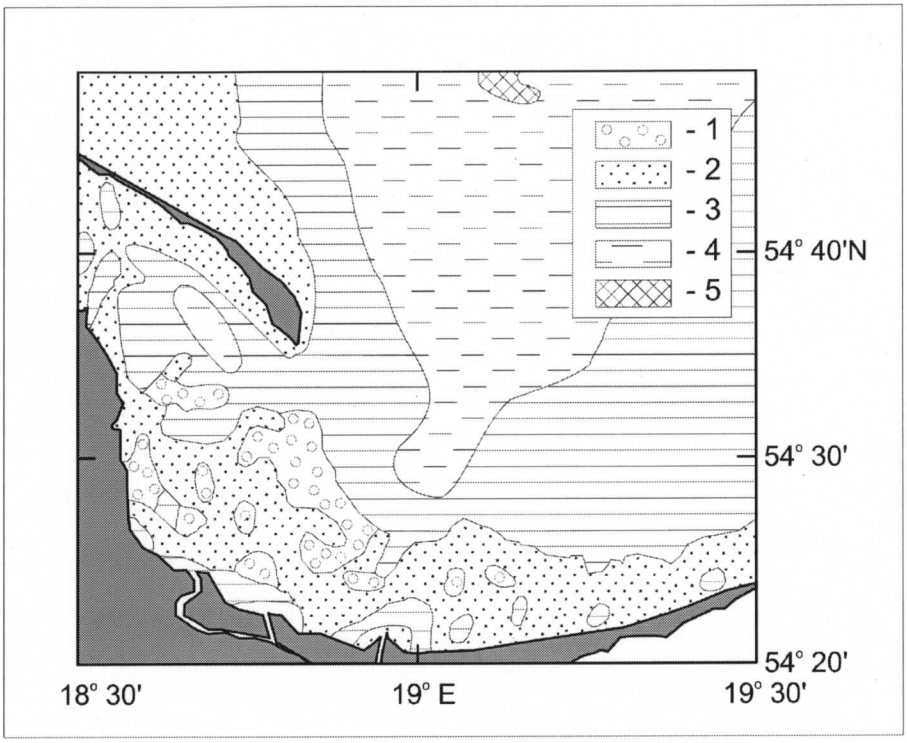

Figure 3.5 Sediment type at Gulf of Gdansk (Figure courtesy of J. Tegowski)

(1 - Gravels, stones; 2 - Sands; 3 - Marine silty clay; 4 - Marine clayey silt; 5 - Glacial marine clay.)

The map of the investigation area is presented in Fig. 3.6. The red circles indicate those measurement points where the transmitting frequencies are about 30 kHz. From Fig. 3.6, we can tell the water depth approximately at different measurement points indicated by the color; and we can use the longitude and latitude of the measurement points to locate them on the map which shows the general sediment type, such as Fig. 3.5.

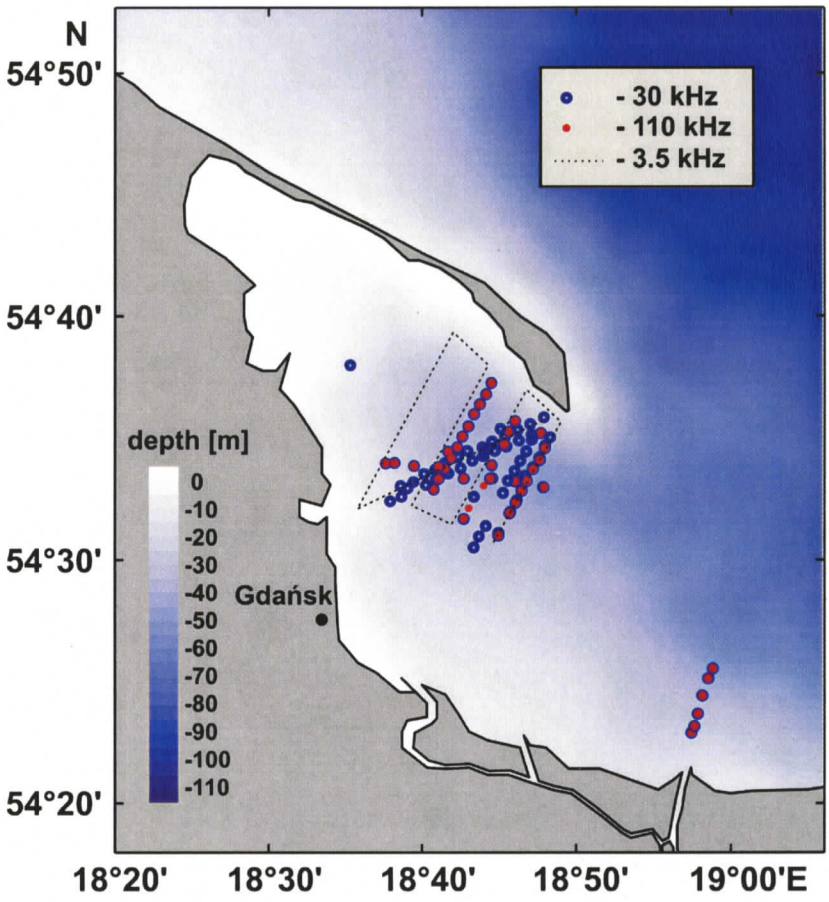

Figure 3.6 Map of investigated area and measurement points at Gulf of Gdansk (Figure courtesy of J. Tegowski)

3.3 System Parameters Settings

In the measurement of nonlinear scattering at gas bubbles in the sediments, the key feature is that gas bubbles are insonified simultaneously by two incident waves at different frequencies.

The transmitting frequencies are chosen based on the following factors:

1) the form of scattering cross section for the sum frequency component of scattered signal which is a function of interval between transmitted frequencies.

2) the resonant frequencies of the transmitters;

3) the possibility of filtering the recorded signals.

The difference between incident wave frequencies can not be large. For a small interval between transmitting frequencies, the scattering cross section for nonlinear components has a strong maximum located in the vicinity of the center between two transmitting frequencies. Increasing this interval causes a strong decrease and spread of resonant peak. When the interval is big enough, the central peak will be divided into the two separated peaks. In consequence, the contribution for the scattered signal is coming from gas bubbles having bigger range of radius.

As to the second factor, when the difference between transducer resonant frequency and used measurement frequencies is too large, the efficiency of the radiating system is too low for nonlinear generation in the gas bubbles.

Considering the filtering process, too small interval between incident wave frequencies is not appropriate because of the difficulty in filtering the echo signal components. The registered band-pass width is associated with radiated pulse length τ ($\Delta f=1/\tau$). The consideration of mentioned effects determines that if the transmitting pulse width is 0.5 ms, then the minimum interval of two emitted frequencies is 1 kHz.

These transmitting frequencies used in the project are:

$f_1 = 30200$ Hz;

$f_2 = 33400$ Hz.

The pulse width is chosen as:

$\tau = 0.5$ ms.

The pulse width is long enough to allow gas bubbles to reach resonance at steady state based on the estimated quality factor of around 10.

During the experiments, acoustic pulses were transmitted every 1 second. Used frequencies made it possible to measure bubble concentration using sum of different components, where resonant frequency is approximately equal to the arithmetical average of transmitting frequencies.

3.4 Calibration of Measurement System

The main goal of the calibration was to

1) determine the hydrophone sensitivity for echo signals at all observed frequencies;
2) determine the acoustical pressure amplitudes generated by transmitters at a distance of 1 m from the transducers.

The calibration was made in open calm sea conditions, the calibration tank at Naval Academy in Gdynia, and at the calibration tank at Technical University of Gdansk. The calibration scheme is presented in Fig. 3.7. The measurement frame with the transducer and calibration hydrophones (B&K 8104 and 1089D made by International Transducer Corporation) were located about 7.5 m below the water surface. Acoustical axes of the transducers were perpendicular to the water surface.

The echo signals scattered at the water surface were registered at the calibration hydrophone on the right, with known sensitivity values, while at the same time, registered at the calibration hydrophone on the left, with the sensitivity values to be determined. The pressure of the backscattered acoustical wave will be the same for both hydrophones. The distance from the sound source to the hydrophones was about 15 m, and the hydrophones were

considered to be in the far field of the source, for the condition $r > \pi D^2 / 4\lambda$ was satisfied, where D is the diameter of the transducer.

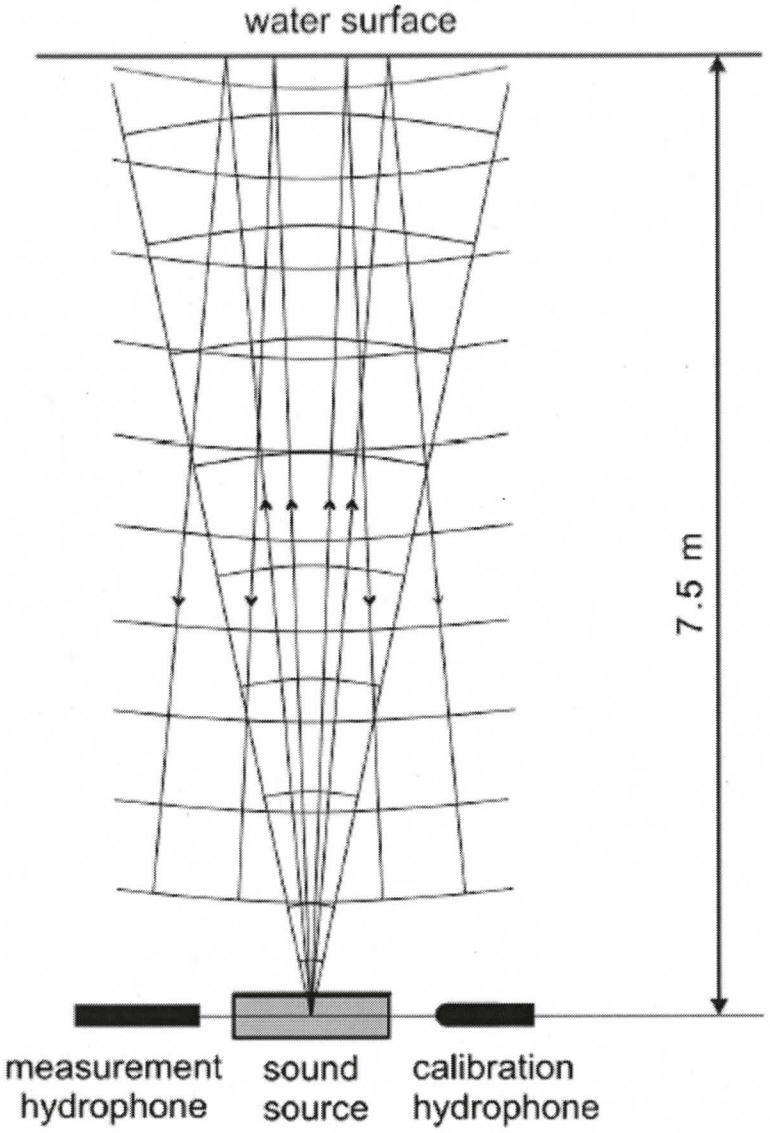

Figure 3.7 Calibration scheme for nonlinear measurement system
(Figure courtesy of J. Tegowski)

Figure 3.8 shows the echo envelopes of 30.2 kHz signals scattered at the water surface, registered by the measurement hydrophone and calibration hydrophone. Output voltage of the power amplifier was 110 V.

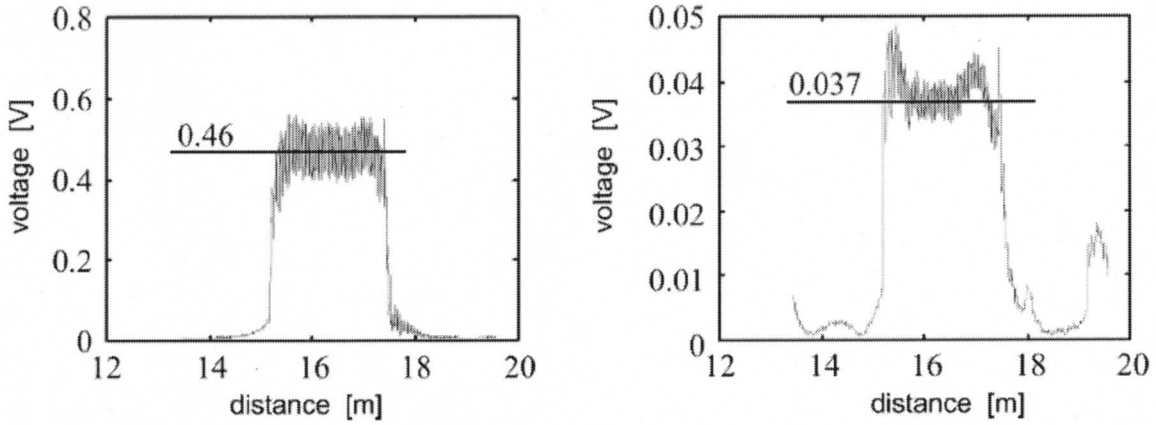

Figure 3.8 Echo envelopes of signal scattered at the water surface - registered by the measurement hydrophone (left figure) and the calibration hydrophone (right figure). (Figure courtesy of J. Tegowski)

Sensitivity of the calibration hydrophone for the frequency used was known as

$$k_c = \text{-206 dB re 1 } V/\mu Pa\,.$$

In the linear scale this sensitivity value is equal to $k_c = 50.12\ \mu V/Pa$.

Then the backscattered wave pressure amplitude at both hydrophones was calculated using the voltage measured at the calibration hydrophone and its sensitivity value:

$$P_r = \frac{U}{k_c} = \frac{0.037V}{50.12\,\mu V/Pa} = 738.25Pa\,. \tag{3.1}$$

Thus the sensitivity of measurement hydrophone was

$$k_m = \frac{U}{P} = \frac{0.46V}{738.25Pa} = 623\,\mu V/Pa\,. \tag{3.2}$$

Conversion of pressure amplitude to a distance of 1m gives the pressure at 1 m from the transmitter P_0 as

$$P_r = P_0 \frac{\exp(-\alpha r)}{r} \tag{3.3}$$

where $\alpha = 0.002$ dB/m, based on the low salinity level of about 7.0 promilles in the Baltic Sea. Thus we obtain the pressure $P_0 = 11.147$ kPa.

Using this approach, the sensitivity values for the hydrophone at different frequencies were obtained in the calibration system as summarized in Table 3.1:

Table 3.1 Hydrophone Sensitivity at different frequencies

	f1	f2	2*f1	f1+f2	2*f2	f1-f2
Hydrophone Sensitivities (μV/Pa)	160	350	440	600	550	520

As for the pressure 1m from the transducer in nonlinear measurements, we use a similar approach to the example illustrated above for a calibration system, but we need to take the wave attenuation in the sediments into account, which is taken as

$$P_{sr} = P_{si} \frac{\exp(-2\alpha_s r_s)}{r_s^2} \tag{3.4}$$

where r_s is the path length of the acoustic wave in sediments; α_s is the pressure attenuation coefficient at different frequencies; P_{si} and P_{sr} are the incident and backscattered wave pressure at sediment surface.

Chapter 4

Echo Data Processing

Based on the nonlinear acoustic scattering theories and experimental setup described in previous chapters, the echo signal processing and inversion process are presented in this chapter, with the results of bubble density profile analyzed and interpreted.

4.1 Data Processing Scheme

During the experiments, the pressure signals of the backscattering acoustic waves were captured at the hydrophone. The numerical processing scheme of these pressure signals is presented in Fig.4.1.

As shown in Fig.4.1, the pressure signals captured at the hydrophone first pass through the signal amplifier. Then the amplified echo signals are converted to digital signals by the 16 bit A/D converter, and recorded in the computer storage system. Since the spectrum of the echo signals may contain both linear and nonlinear frequency components, in order to measure these spectral components separately, the received signal went through a band-pass filter, where the bandwidth is taken as half of the difference between two primary transmitting frequencies $\Delta f = |f_1 - f_2|/2$. The backscattered signal envelopes were obtained by applying a Hilbert transformation to the filtered signals, where a moving average process was employed to smooth the shape of the envelopes. In the final step, the inversion process was implemented based on the calculated

values of scattering volumes as well as the calibration data for gas bubbles concentrations.

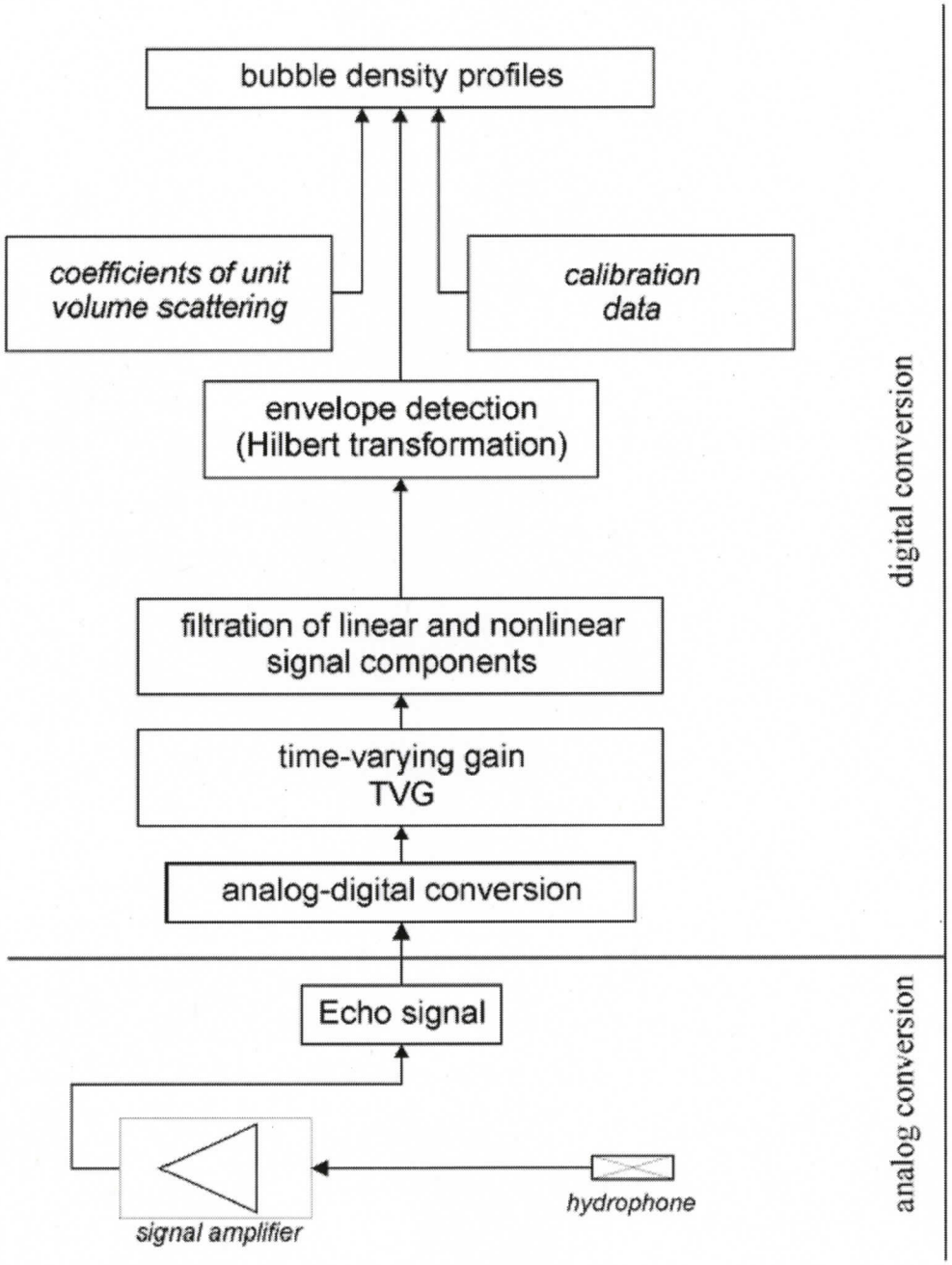

Figure 4.1 Data processing scheme of nonlinear measurement system (Figure courtesy of J. Tegowski)

4.2 Echo Signal Pre-processing

The data available for processing were the digitized echo signals recorded in the computer systems during the experiments. A typical raw data file is shown in Fig. 4.2., and consisted of ten consecutive pairs of signals which were sampled at 500 kHz.

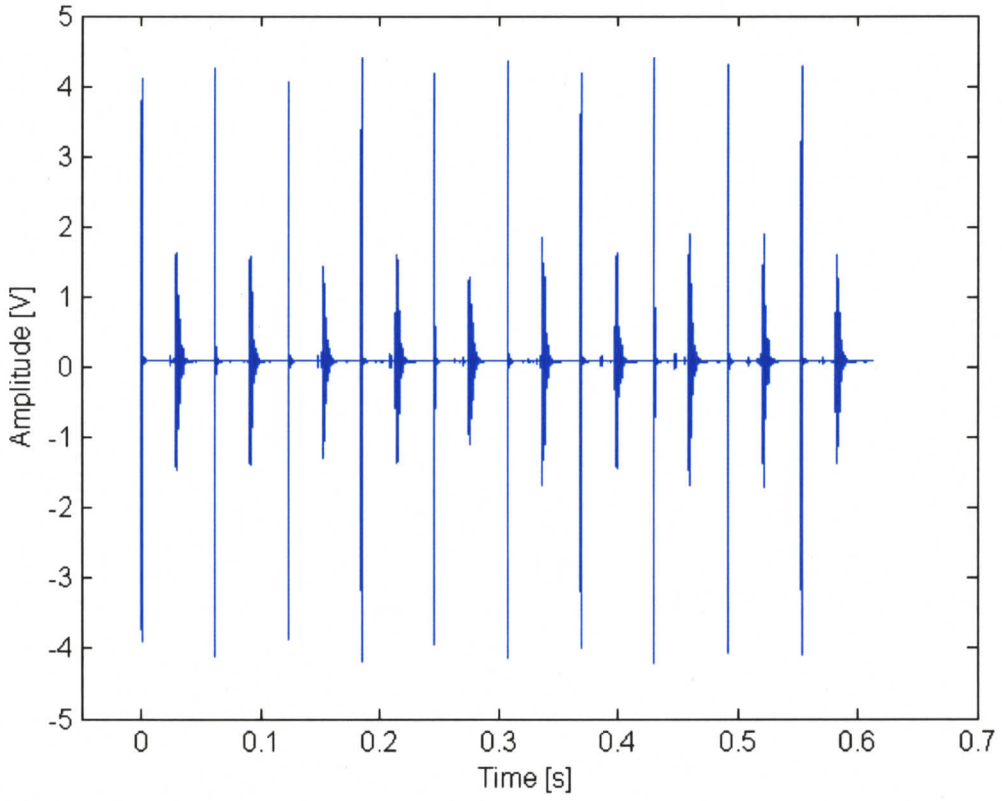

Figure 4.2 Ten Consecutive transmitting pulses and echoes from the bottom. (Transmitting frequencies are 30.2 kHz and 33.4 kHz)

The transmitted pulse width was 0.5 ms, and the interval between two transmitted pulses was about 0.06 s. At each measurement point, a total of 500 pulses were transmitted and 500 echo signals were recorded and saved in 50 data

files, with each data file containing 10 consecutive pulses and echoes as shown in Fig.4.2.

If we pick out a single pair of echo signals, as shown in Fig.4.3, we can see a strong narrow pulse, which is the direct path signals captured by the hydrophone, for the transmitted pulses at frequencies 30.2 kHz and 33.4 kHz. The subsequent pulses with smaller amplitude and longer duration are the echo signals backscattered from the ocean bottom. Between the direct path signals and echo signals from the ocean bottom, sometimes there are signals showing up in the data file. These could be from biological scatterers such as fishes.

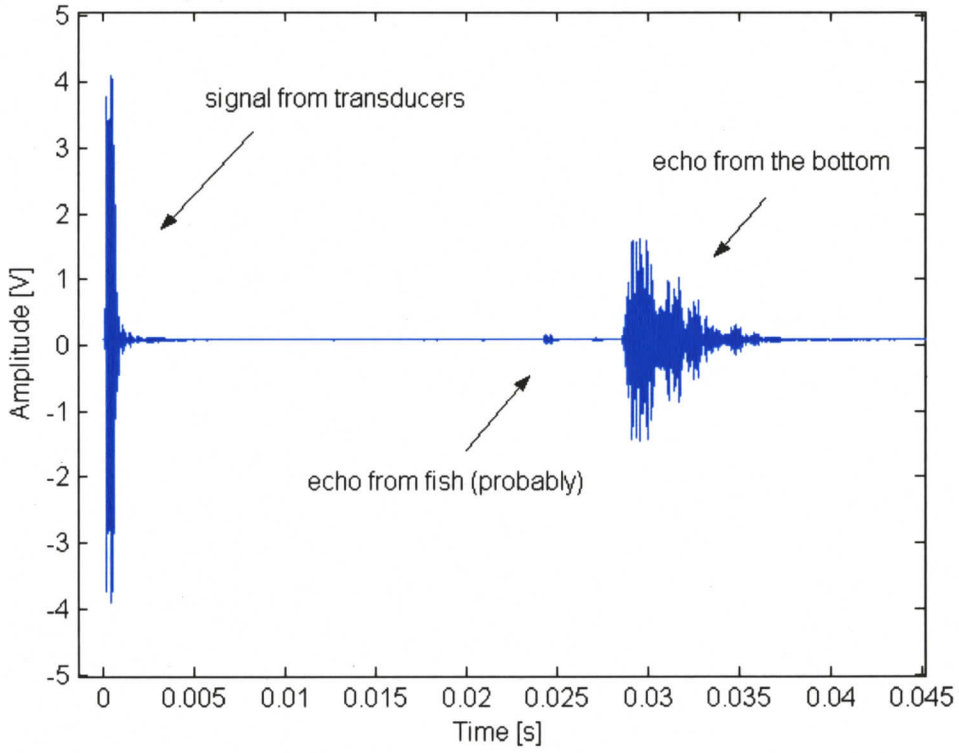

Figure 4.3 Detailed visualization of elements of recorded signals

If we divide one data file equally into ten pieces, then each piece will contain one direct path signal and one bottom backscattered echo signal as shown in

Fig.4.3. We assume the start of each piece of the data file as zero in time, and then apply a time window to each piece of data, with the same window length and at the same location relative to the zero for each piece of data, to eliminate the direct return signal. We then obtain ten isolated echo signals, as shown in Fig.4.4, which are all from the same data file, for example, data file "helgdy_7_0.001".

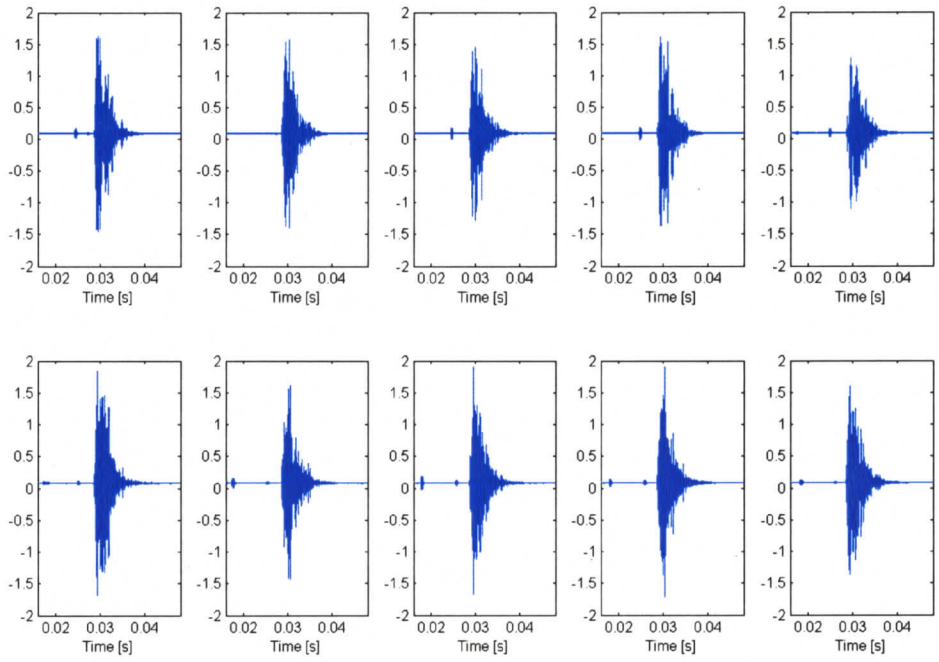

Figure 4.4 Ten consecutive isolated echo signals (from one data file)

During the experiment, the vessel was drifting, which leads to the variations in different echo signal strength as shown in Fig.4.4.

In Fig.4.4 there are offset signals whose strength is about 0.09V, which might be caused by the electronic circuits. The offset signal needs to be removed before we calculate the echo spectrum, or a high-pass filter needs to be used to eliminate the noise in the lower band, which are generated by the offset in calculating the spectrum.

In the next step, the spectrum of each echo signal was calculated, and Fig.4.5 shows the averaged echo spectrum over 10 consecutive echo signal spectra from those shown in Fig.4.4.

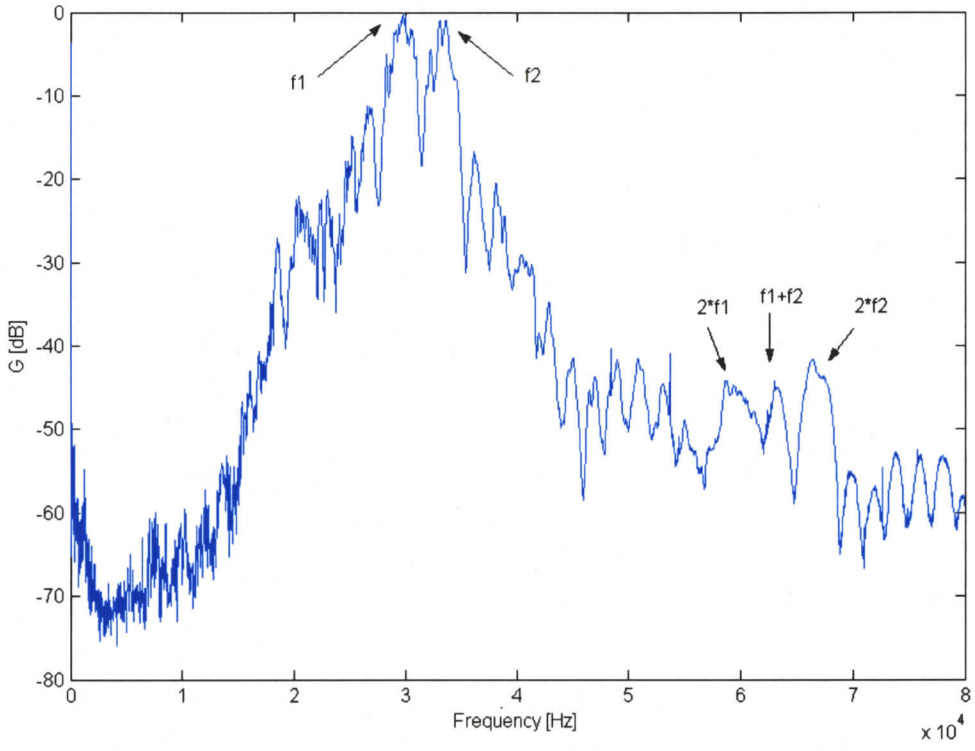

Figure 4.5 Averaged spectrum of 10 consecutive echoes in one data file

From the averaged spectrum in Fig.4.5, we can see there are two obvious peaks at the transmitting frequencies $f_1 = 30.2\,\text{kHz}$ and $f_2 = 33.4\,\text{kHz}$, and there are smaller peaks, but still very obvious, at nonlinear frequencies of $2f_1 = 60.4\,\text{kHz}$, $f_1 + f_2 = 63.6\,\text{kHz}$, and $2f_2 = 66.8\,\text{kHz}$. The nonlinear components are -40 ~ -50 dB lower in signal strength compared to the linear components, but they are still well observed in the spectrum of the echo signals. As a comparison, the signal at $|f_1 - f_2| = 3.2$ kHz is not obvious in the spectrum since it is buried in the noise at the lower frequency band. This echo spectrum confirms the

nonlinear backscattering theory described in Chapter 2 that the echo signal at $f_1 + f_2$ will be much more useful than the echo signal at $|f_1 - f_2|$ for bubble identification.

In order to get the echo features at the linear and nonlinear frequencies, all the frequency components, which are represented by the peaks in the echo signal spectrum, will be filtered individually.

4.3 Signal Filtering

To obtain the echo signal envelope for each individual frequency, $f_1 = 30.2$ kHz, $f_2 = 33.4$ kHz, $2f_1 = 60.4$ kHz, $f_1 + f_2 = 63.6$ kHz, $2f_2 = 66.8$ kHz, digital bandpass filters were designed and applied to the echo spectrum.

The bandwidth of the bandpass filter was chosen as $\Delta f = |f_1 - f_2|/2 = 1.6\,\text{kHz}$. The filter is designed to implement this narrow passband, together with 50 dB attenuation for the adjacent frequencies. Chebyshev Type II was chosen for the filter design due to its flat response in the passband, which means it is free of passband ripple, and its equiripple feature in the stopband.

Five Chebyshev Type II filters were designed and applied to the spectrum of every single echo signal. The amplitude and phase response of these bandpass filters is displayed in Fig.4.6.

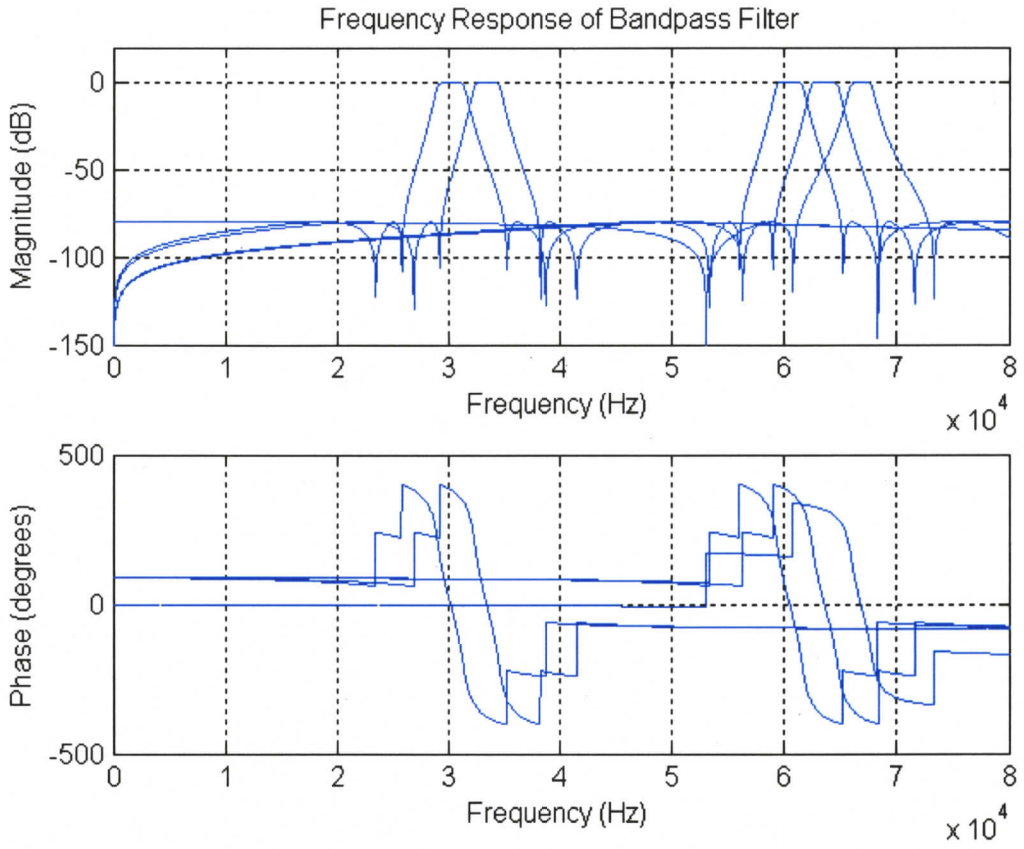

Figure 4.6 Frequency response of the bandpass filters

From the frequency responses of the five different bandpass filters, they all have a bandwidth of 1.6 kHz, which meets our goal. They decrease to –50 dB when reaching the neighboring center frequency of the adjacent bandpass filter. This feature makes sure that the output signal is for a single frequency component. For instance, the first bandpass filter has a center frequency of $f_1 = 30.2$ kHz, with a bandwidth of 1.6 kHz, and its amplitude response at adjacent frequency $f_2 = 33.4$ kHz is -50dB compared to the amplitude at $f_1 = 30.2$ kHz in the passband.

The band-pass filters are applied to every single echo signal. The output signal spectra from each band-pass filter are recorded, as shown in Fig.4.7.

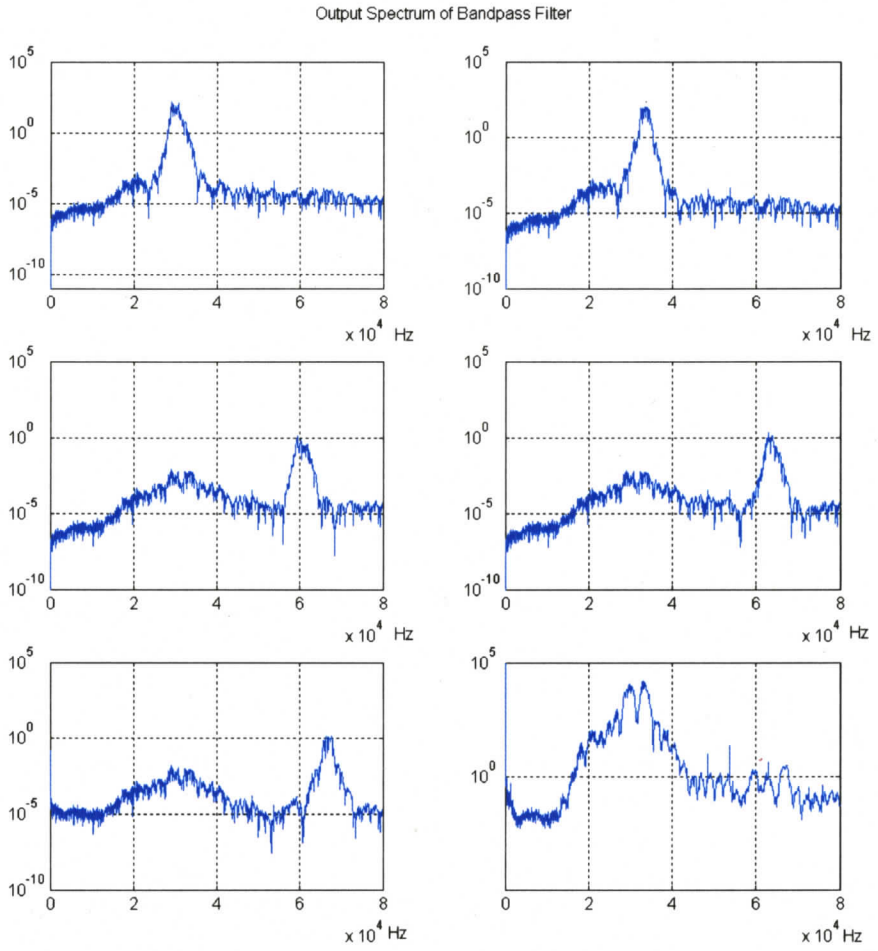

Figure 4.7 Output spectra of the different bandpass filters

Each plot displays one output of the bandpass filter, and each contains only one frequency component. The last plot is the spectrum of the input signal of the filters.

Since the signal strength at transmitting frequencies is much stronger than nonlinear components as displayed in averaged spectra, we also need to make sure that the bandpass filter designed for nonlinear frequency components should eliminate signals at transmitting frequencies f_1 and f_2. As shown in Fig. 4.7, the output of the nonlinear components is about 30 dB stronger than the

suppressed response at transmitting frequencies. Thus the outputs of the bandpass filters for the nonlinear frequencies have negligible interference from the signal at primary frequencies.

These output signals at the nonlinear frequencies will be used for the inversion for bubble concentrations.

4.4 Signal Envelopes Extraction

After separating different spectral components using the filtering process, inverse FFT transform were applied to the positive frequency component of the output spectra, while setting the negative frequency components to zero. Thus, the obtained result of inverse FFT is the analytic signal in the time domain, and then we multiply the result by a factor of two to compensate for the signal energy lost when we set the negative frequency component to zero. This inverse FFT process gives the equivalent result compared to applying the Hilbert transform to the real time domain signals. The modulus of the analytic signal, which is the signal envelope, is used for display and further processing.

These echo signal envelopes at different frequency components provide the time dependence of corresponding amplitudes of the backscattered signals. Their relative positions in time domain, envelope shape, as well as the duration will provide much information about the sediment type, gas presence and concentration etc. which will be analyzed in following paragraphs. Fig.4.8 presents the envelopes of different spectral components for a single echo signal.

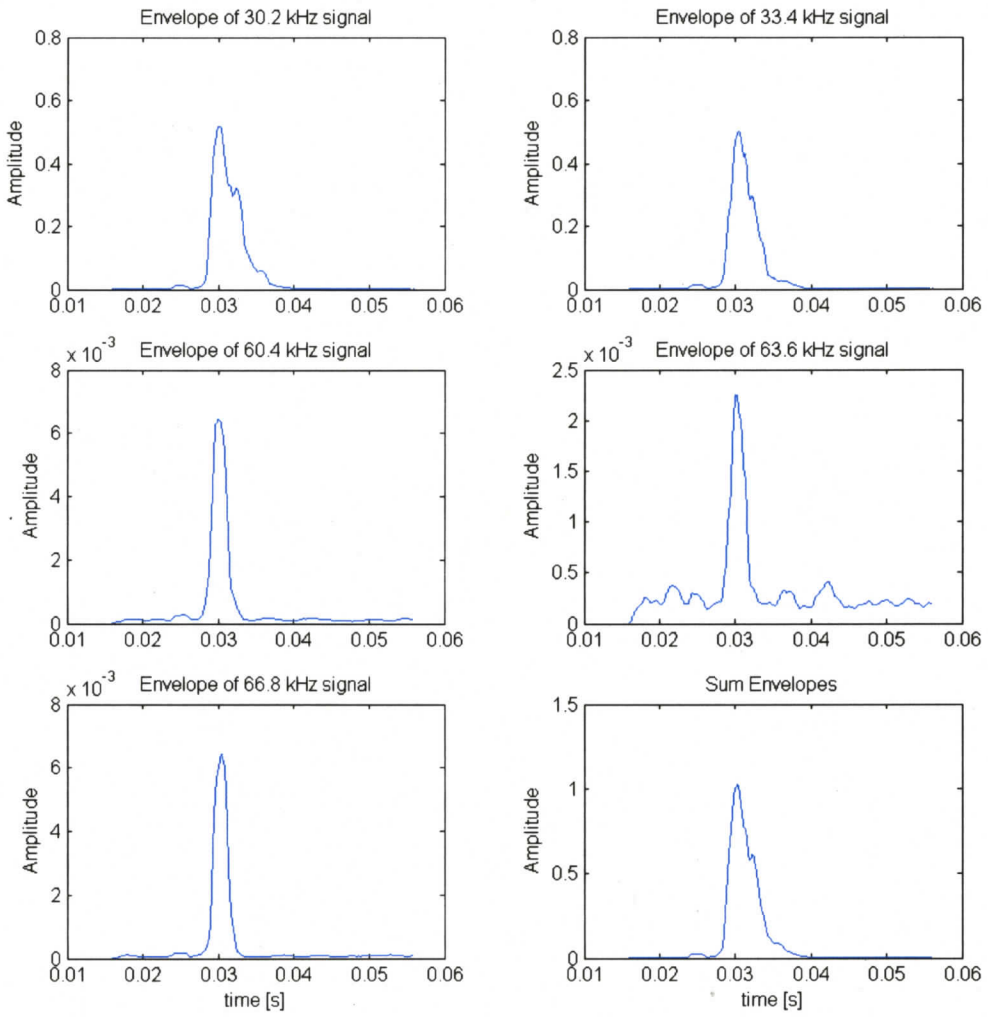

Figure 4.8 Envelopes of different spectral components

A moving average process was applied to smooth the shape of the envelopes. The moving average window length is chosen to be 5000 points, compared to a total length of 20,000 points of the time window chosen for a single echo signal.

From Fig.4.8 we can obtain the following information for further processing:

1) The arrival time and the duration of the echo signals of different spectral components. From this we can determine the depth of sediment surface, and the depth profiles of bubble layers;
2) The signal strengths, or the amplitudes of different spectral components. This information will be used, together with the results from calibration data and computed scattering volume, for the inversion process to obtain quantified values of the bubble concentration.

4.5 Echograms

The echograms will show us the depth profile as well as the backscattered signal strength of different frequency component as a function of depth. Based on the echograms obtained from the available data, the following echograms will display the features at different sites with different sediment types:

Case 1:

Fig.4.9 shows both the linear and nonlinear component for a single echo, and the echogram for 200 consecutive echoes at Lat: 54^0 34′ Lon: 18^0 45′, with the sediment type of sand-silt-clay.

Case 2:

Fig.4.10 shows the single echo and the echogram for 200 consecutive echoes at Lat: 54^0 34′ Lon: 18^0 42′, with the sediment type of marine clayey silt.

Case 3:

Fig.4.11 shows the single echo and the echogram at Lat: 54^0 34′ Lon: 18^0 41′, with the sediment type of marine silty clay.

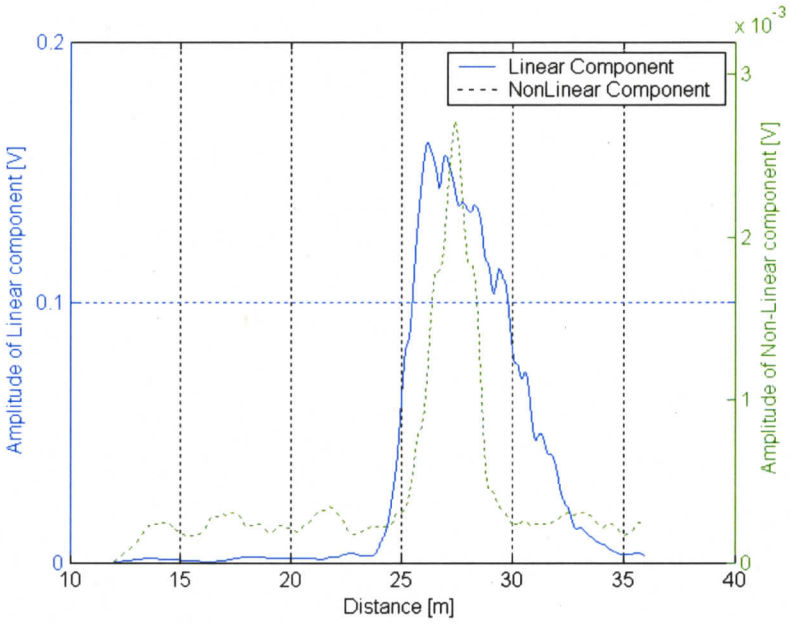

Figure 4.9.a The amplitudes of linear and nonlinear components of a single echo

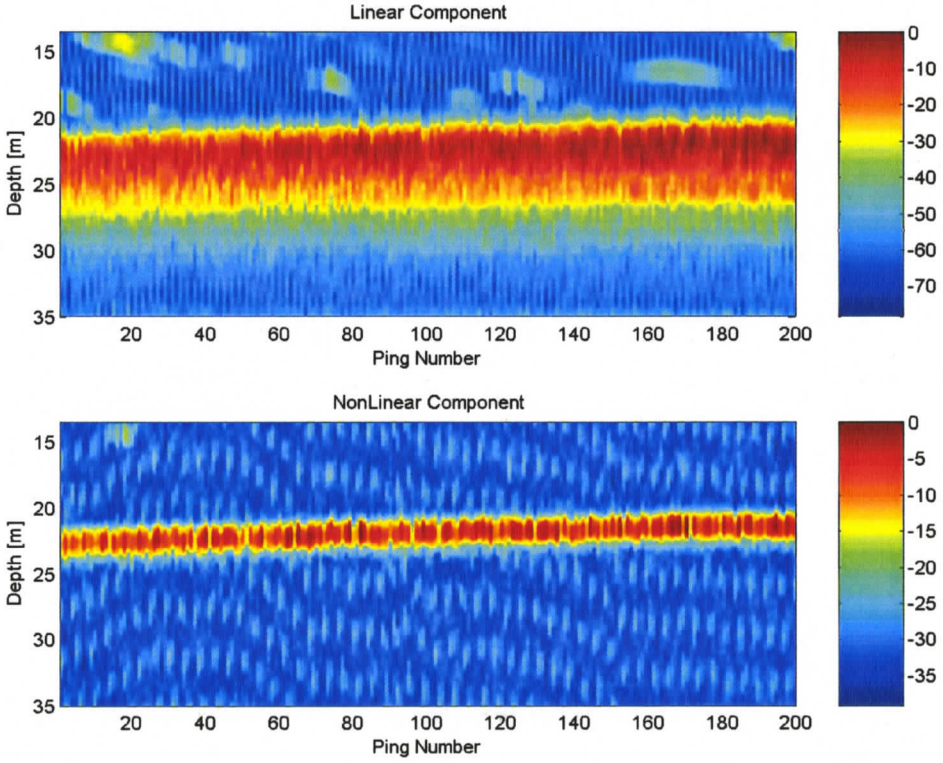

Figure 4.9.b Echogram for consecutive 200 echoes (Lat: 54^0 34′ Lon: 18^0 45′ Sediment Type: Sand-silt-clay.)

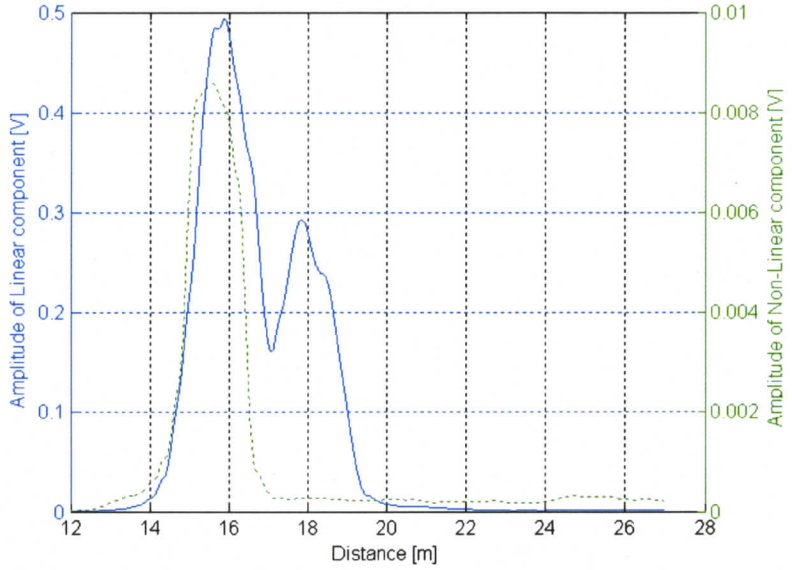

Figure 4.10.a The amplitudes of linear and nonlinear components of a single echo

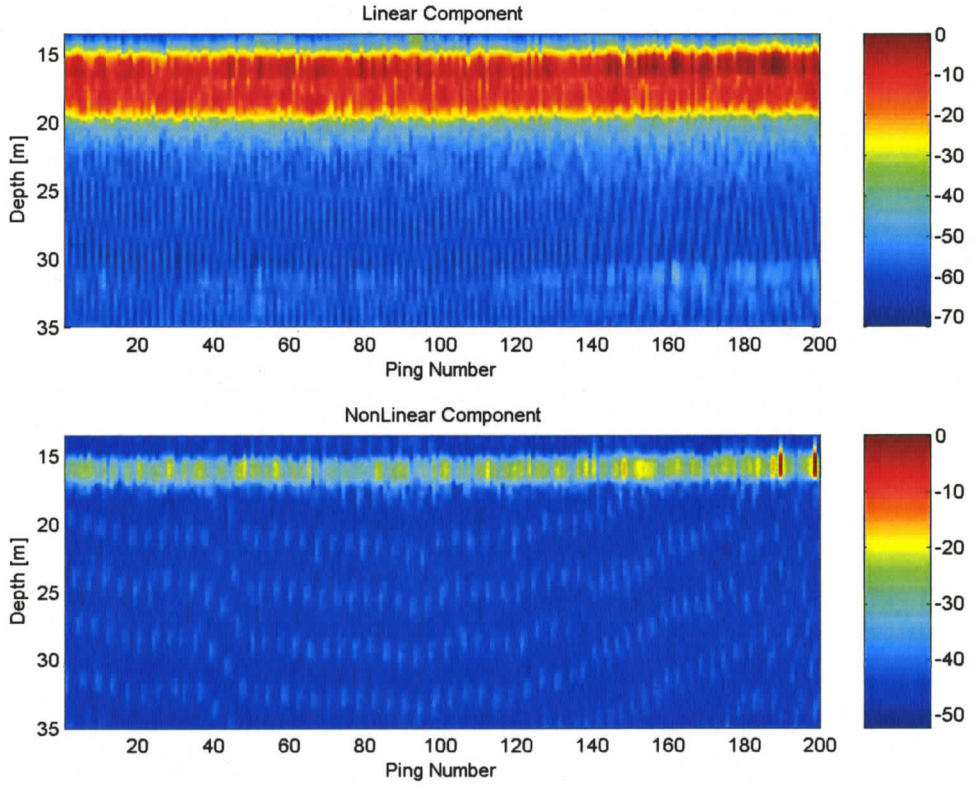

Fig.4.10.b Echogram for consecutive 200 echoes (Lat: 54^0 34′ Lon: 18^0 42′

Sediment Type: Marine clayey silt)

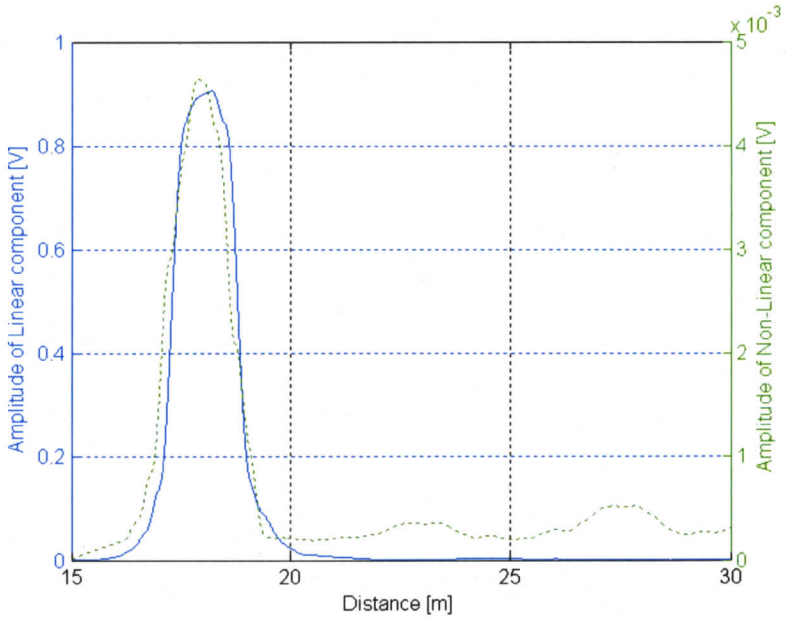

Figure 4.11.a The amplitudes of linear and nonlinear components of a single echo

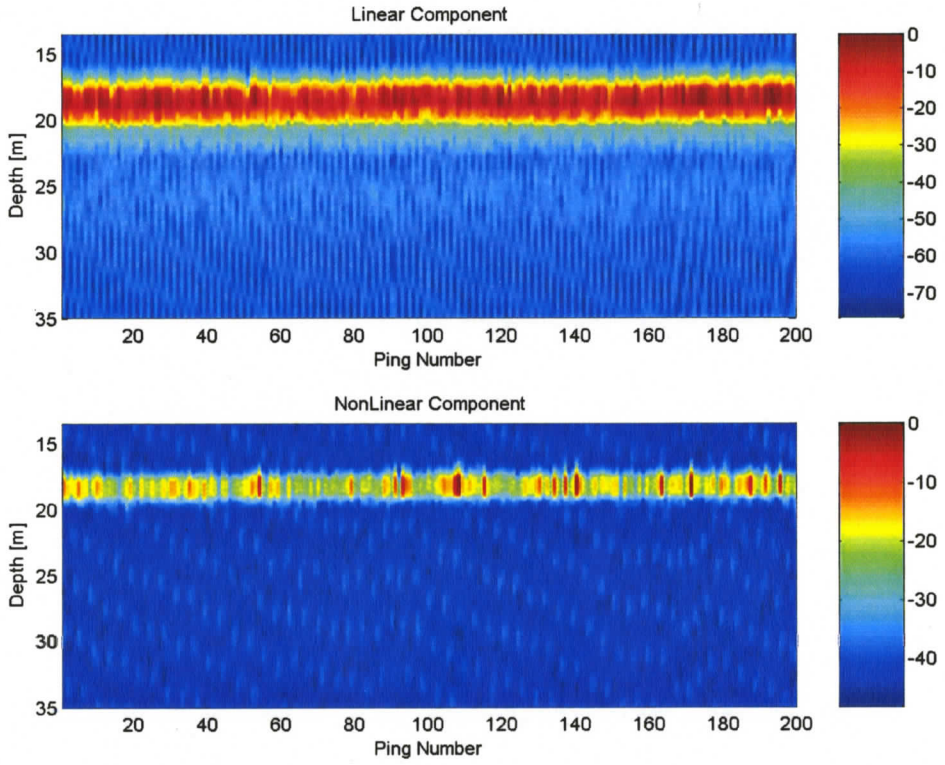

Figure 4.11.b Echogram for consecutive 200 echoes (Lat: 54^0 34′ Lon: 18^0 41′ Sediment Type: Marine silty clay)

Before analyzing the echograms at different sites, a brief discussion of the sediment types and the beam geometry will be given.

These data are sampled at sites with different sediment types. The sediment types are determined by the relative proportion of sand, silt and clay found in a given sediment type. Sand is gritty and the individual grains or particles can be seen with the naked eye. The sediment will be relatively coarse if the sediment is predominantly sand. Silt is smooth when wet, and the individual particles of silt are much smaller than those of sand, and can only be seen by microscope. Clay is sticky and elastic-like when wet. The sediment may contain all of these grains with different sizes, but their proportion determines the type. The physical and geoacoustic properties of the different sediment types have been studied for different areas (Bachman 1989). But no measured properties are available for the Gdansk area as yet.

The beamwidth of the hydrophone at the sum frequency is determined by the geometric size of the hydrophone as well as the frequency. Based on the directivity function of a circular source, the beamwidth is calculated for each of the frequencies.

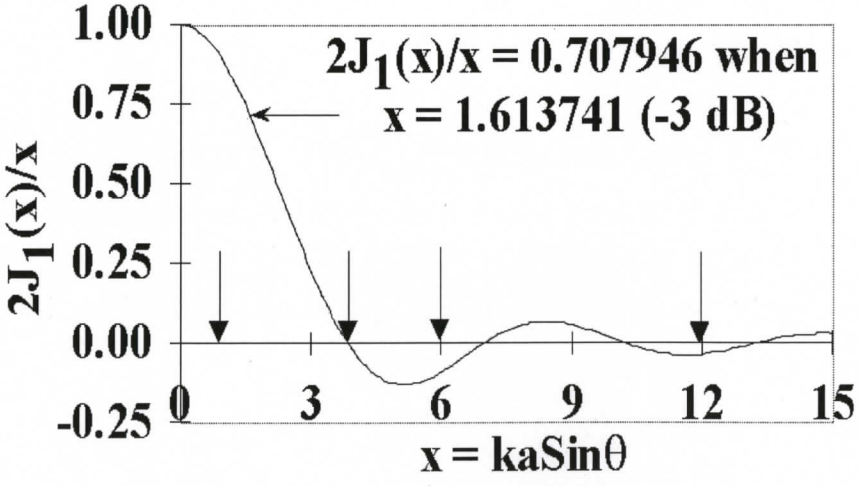

Figure 4.12 Directivity function of a circular source

Table 4.1 Half beamwidth for circular sources at different frequencies

Frequency	a (Radius of Circular Source)	k (wave number)	sinθ (θ is the half beamwidth)	θ (in degrees)
30.2 kHz	0.08m	126.4	0.1595	9.2^0
33.4 kHz	0.08m	139.9	0.1441	8.3^0
63.6 kHz	0.06m	266.4	0.1009	5.8^0

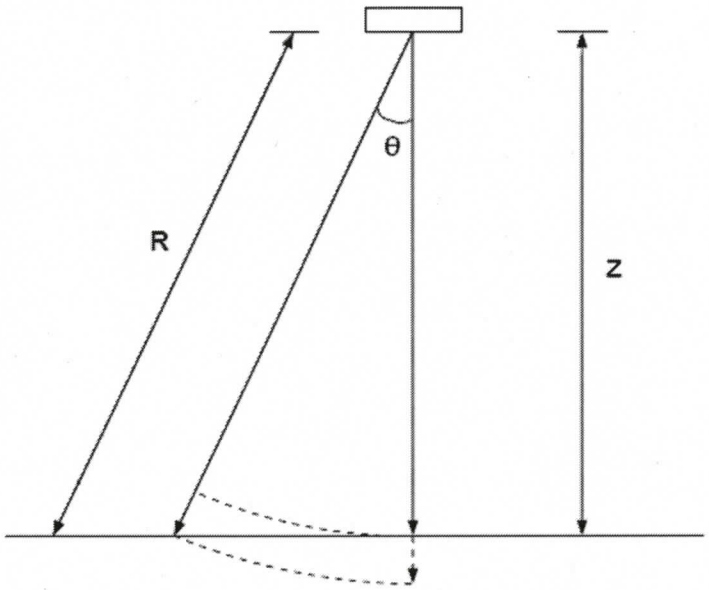

Figure 4.13 Interaction of the beam of the hydrophone with sediment surface

In Figure 4.13, *R* is the distance along the edge of the beam, *z* is the distance from the transducer to the sediment surface. From the echograms, *z* is 20 - 30m, so for the sum frequency, the time difference between arrival time from middle of the footprint to the edge of the footprint is $2(R - z)/c = 2\ z\ (\cos^{-1}\theta - 1) \approx 0.17$ms, which is less than the transmitting pulse width 0.5ms. The whole surface area of footprint is insonifed within the transmitting pulse duration.

The comparison of signal envelopes for the linear component at 30.2 kHz and the nonlinear component at 63.6 kHz is demonstrated in Fig. 4.9.a, Fig. 4.10.a, and Fig. 4.11.a. The echograms of consecutive 200 pulses in Fig. 4.9.b, Fig. 4.10.b, and Fig. 4.11.b, display a full view of the echo signal at linear and nonlinear frequencies over time.

There are some common features in the three cases. First there is about 30 dB difference in signal strength between the two components, which has been determined by the difference in the scattering cross sections at two different frequencies. Second, some features of sediments can be determined by the echo signal envelope of both linear and nonlinear components:

- *Envelope Duration.* The linear signal envelope duration is an indication of the penetration depth of the incident wave into the sediments. The time at the rising edge of the envelope provides the depth of the water-sediment interface. But for the nonlinear signals, since they are generated by the oscillating bubbles, their envelope duration represents the depth of the gas layer in which the bubbles are resonating at the transmitting frequencies.

- *Envelope Amplitude.* The signal strength at the rising edge of the linear signal envelope demonstrates the backscattering strength from the water-sediment interface. The peak of the nonlinear signal envelopes represents the signal strength at nonlinear frequencies generated by the bubbles at a specific depth.

- *Envelope Shape.* The shape of the envelope can be useful in many situations for seabed classification. For this project, the linear signal envelope displayed various shapes, such as in Fig. 4.9.a, Fig. 4.10.a, and Fig. 4.11.a, which may be due to different sediment types. But we care more about the envelope shape for the nonlinear component. For different cases, the nonlinear signal envelopes are

showing unique peaks, and monotonic rising amplitude before the peak and monotonic falling amplitude after the peak value.

- *Relative Positions of Linear and Nonlinear Envelopes.* The relative positions for linear and nonlinear components can provide some clues about the sediment types as well as the gas layer position. For Fig. 4.9, the nonlinear component comes later than the linear component, which may due to that the linear echo component comes from the volume and surficial scattering at the top sandy sediment, while the nonlinear component echo comes from the muddy layer placed below the sandy layer which can act as a barrier for the gas bubbles. For Fig. 4.10, the nonlinear component comes a little earlier than the linear component, and the peak of nonlinear component coincidences with the first peak of the linear component, which may due to that the nonlinear component envelopes are the effect of scattering at the thin layer of top muddy sediment. For Fig. 4.11, the envelope shapes for linear and nonlinear components are almost the same, which may due to that the muddy sediments are on top of the sandy layer, and gas bubbles exist in the muddy layers.

It has been a very active research area to determine the physical and acoustical properties of the sediments at high frequencies from the echo signal envelopes (Stanton 1986, Sternlicht 2003). The determination of the sediment properties based on the echo envelopes is actually controlled by many factors such as the roughness of the sediment surface, the acoustic beamwidth, the angle of incident waves, the sediment volume scattering properties etc. Using a single envelope it is hard to determine the sediment properties due to that different sediment types might have caused echo signals with similar shapes under different situations. Sternlicht (2003) has used average echo envelopes to determine the mean grain size, interface roughness spectral strength, and

sediment volume scattering coefficient. Biffard (2005) has used signal echo durations to classify sediment types.

Apparently there are ambiguities in the sediment properties based on the echo signal parameters. But the introduction of both linear and nonlinear signal component will reduce the ambiguity due to more information provided by the envelopes of the nonlinear echo signals which come exclusively from the gas bubbles in the sediments. How to combine the linear and nonlinear components to produce a more accurate prediction of sediment physical and acoustical properties deserves further research.

4.6 Inversion for Bubble Density Profiles

4.6.1 Simplified Calculation Algorithm of Scattering Volume

Based on the geometry of the experimental setup, the distance between the transducer and the hydrophone is 8 cm on both sides, which is much smaller than the water depth of 20~30 meters where the data was collected. From Table 4.1, it is very obvious that the hydrophone between the two transducers at nonlinear frequency has the most narrow beamwidth.

So an assumption was made for the calculation of the scattering volume that the common area of the three beams by the two transducers and the hydrophone will be solely determined by the beam of the hydrophone. This will make the calculation much simpler for scattering volume given the pulse width and water depth.

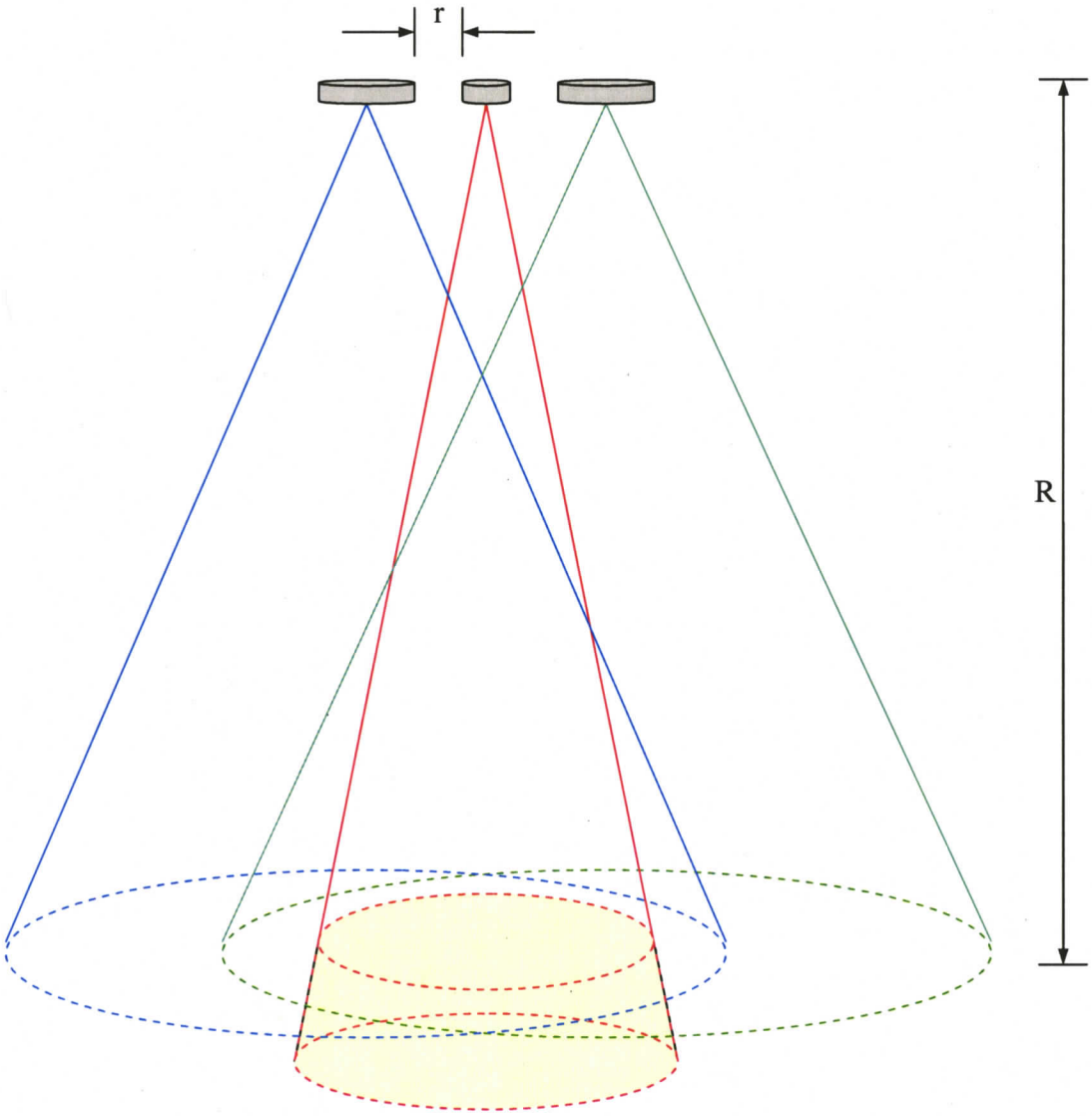

Figure 4.14 Simplification of scattering volume calculation

4.6.2 Bubble Density Profile Inversion

Based on the nonlinear acoustic scattering theory described in chapter 2, the inversion will be implemented according to Equation 2.62.

The ratio of the echo signal intensity to the incident wave signal intensity on the left side of the equation was calculated based on the square of the ratio of echo signal amplitude in Volts to the transmitting signal strength in Volts.

The distance R is determined by the echo arrival time assuming the sound wave velocity of 1500m/s in the sea water. The scattering volume was calculated based on the simplified algorithm described in the previous section.

The bubble density profiles and corresponding echograms are demonstrated in Figure 4.15.

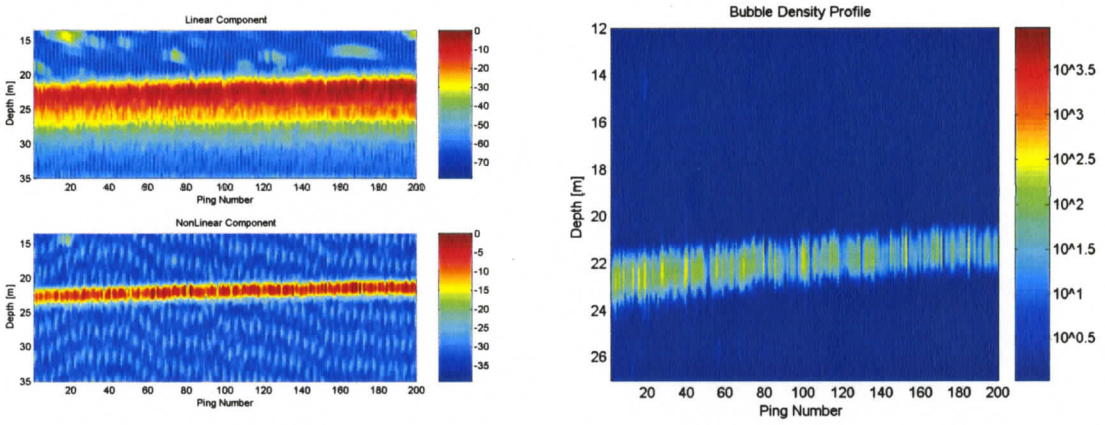

Figure 4.15.a Echogram and bubble density profile at Lat: 54^0 34′ Lon: 18^0 45′

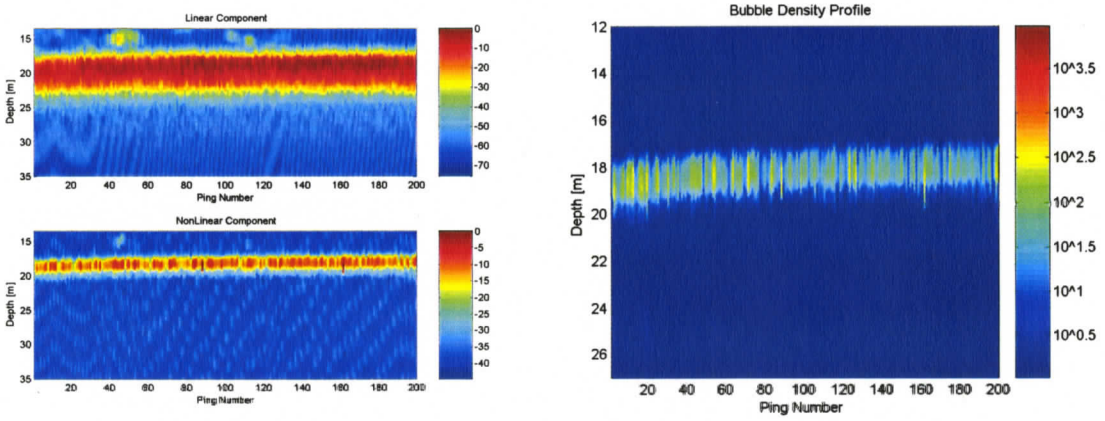

Figure 4.15.b Echogram and bubble density profile at Lat: 54^0 34′ Lon: 18^0 45′

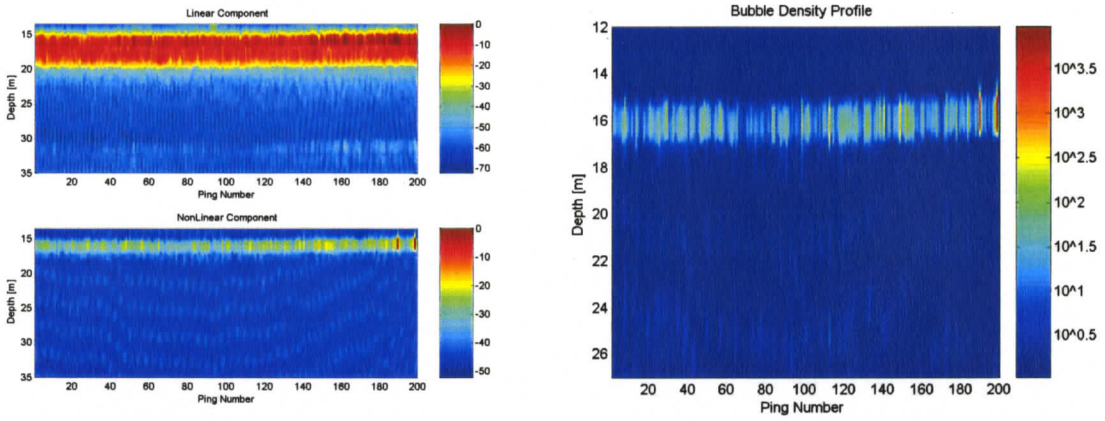

Figure 4.15.c Echogram and bubble density profile at Lat: 54^0 34′ Lon: 18^0 42′

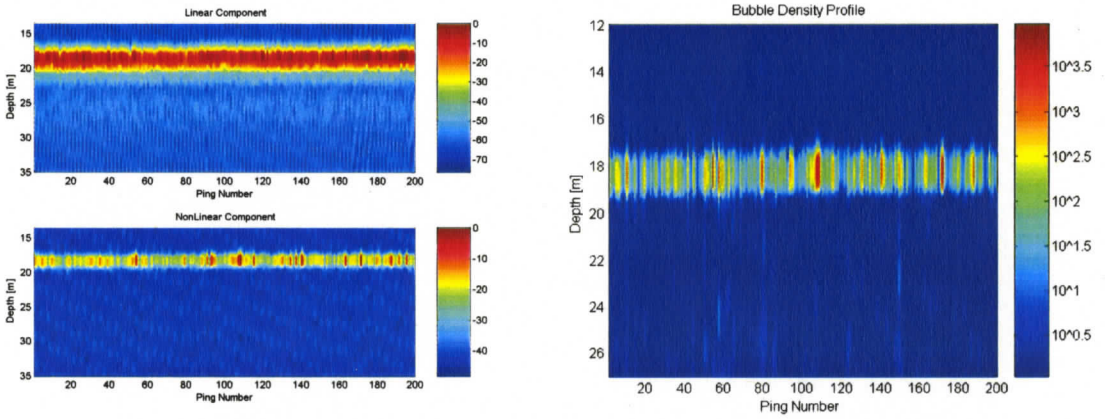

Figure 4.15.d Echogram and bubble density profile at Lat: 54^0 34′ Lon: 18^0 41′

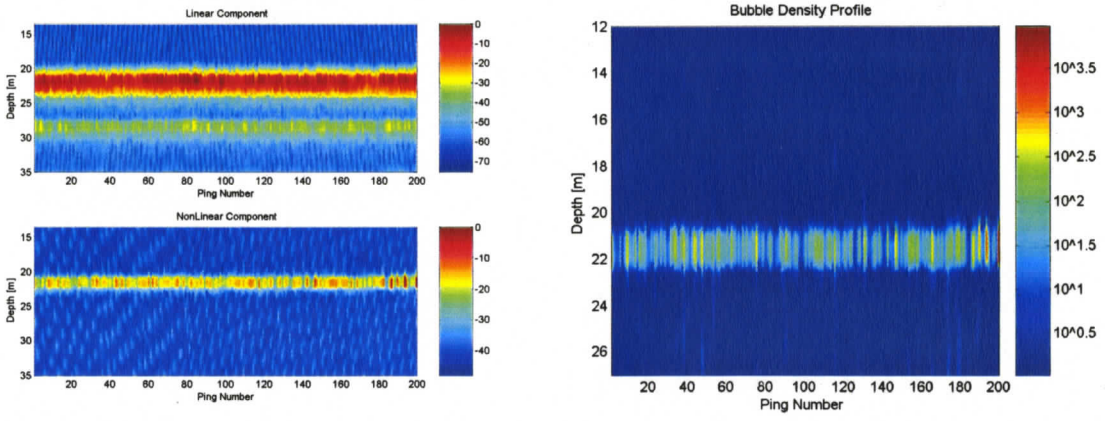

Figure 4.15.e Echogram and bubble density profile at Lat: 54^0 33′ Lon: 18^0 39′

The bubble density profiles in Figure 4.15 show the number of bubbles in the surface layer of the sediment per cubic meter per a radius range of 1μm. These results indicate the existence of gas bubbles in the surface layers of the sediments at Gulf of Gdansk; their distribution is about 2~3 m near the sediment surface; as well as their abundance at different locations. The results of the measurements show that the resonant gas bubble concentrations varies from 0 to 10^3 $m^{-3}\mu m^{-1}$. The results also demonstrate that for most investigated areas, there are hundreds or thousands of gas bubbles in the sediments resonating at transmitting frequencies of the nonlinear measuring system and generating the nonlinear responses at the sum frequency.

From the results of bubble densities, we can also get a rough estimate of the gas fraction for the specific size of gas bubbles in the sediments. For a nonlinear acoustic measuring system with transmitting frequencies of 30.2 kHz and 33.4 kHz, and a water depth of around 25~30 meters, the radius of the bubbles that will generate backscatter signal at the nonlinear frequency 63.6 kHz will be around 0.2mm. Thus for the gas bubbles whose radius fall in a range of 1μm centering at 0.2mm, the gas fraction will be 3×10^{-11} ~ 3×10^{-7} per cubic meter in the sediment.

From Figure 4.15.a and 4.15.b, the data were taken at very close locations. The echograms at the linear frequency show some scatterers above the sea bottom, which could have been some plants or fishes. As a comparison, the echogram at nonlinear frequency display no scatterer or very weak scatterers at corresponding depth, which suggests that the nonlinear signal comes solely from the gas bubbles instead of some other scatterers near the sea bottom.

Figure 4.15.c, 4.15.d and 4.15.e display the bubble density profiles for another three locations which are further from the two in 4.15.a and 4.15.b. The

bubbly layer has a depth of about 2 meters, while the linear signal has different penetration depth into the sea floor. The thickness of muddy sediment in most areas of Gulf of Gdansk is between 3 m and 6 m (Tegowski, 2006), where the gas bubbles from the migration of methane from the deep bottom gassy layers reside.

Chapter 5

Conclusion

In this thesis, a new nonlinear acoustic remote sensing technique is applied to measure the existence, distribution and concentration of gas bubbles in the Gulf of Gdansk, where the bottom sediments are known to be rich with gas bubbles in the surface layers of sediments. The main reasons for the existence of gas bubbles in this area is from the originated bacterial decomposition of organic matter as well as the migration of methane form the deep bottom gassy layers. The nonlinear method used in the detection of gas bearing sediments is based on the fact that gas strongly changes the acoustic properties of the sediments, and the nonlinear acoustic scattering theories that were developed to describe the nonlinear scattering behaviors of the gas bubbles in sediments.

The experiment was designed based on the nonlinear scattering theory, with the transmitting frequencies carefully chosen considering the factors, such as the size of gas bubbles of interest, the form of the scattering cross section as well as the processing of echo signals etc.. Bandpass filters were designed to separate the individual frequency components. The output signals from the bandpass filters were passed through a Hilbert transform to obtain the signal envelopes in time domain. These signal envelopes, together with the calculated scattering cross section, the scattering volume, and the calibration data, were all used to invert for the bubble density profile according to the acoustic nonlinear scattering theory for gas bubbles.

The results of gas bubble density profiles prove the validity of this nonlinear acoustic measuring method due to its capability of detecting the presence and measuring the distribution and concentration of the gas bubbles.

The main advantages of this method are obvious. First of all, as an acoustic remote sensing technique, the method brings the fact that the bubbly medium is undisturbed by the intrusion of the equipment, and it provides continuous data over a large area instead of sparse data collected by in-situ samples.

Secondly, the method of nonlinear acoustic measurement is very helpful to determine the gas bubble concentration in the water body and in the upper layer of sediments. The appearance of nonlinear component, the sum frequency in this application, in the echo signal enables us to distinguish between bubble and non-bubble scattering.

Thirdly, it is a promising tool in the remote sensing the free gas presence, remote control of gas emission from sediments during drilling, or the ecological monitoring of methane or sulphuretted hydrogen presence in the top sediment layers.

The disadvantages with the nonlinear acoustic method are that the axial extent is limited by the windowing procedure; the cross-sectional extent depends on the divergence of the sound beam and the range. Therefore the backscatter comes from a spherical cap which covers more than one depth. Since the bubble populations are sensitive functions of depth, the divergence of the beam produces an undesirable averaging over a range of depths. Besides, it is necessary to correct for the attenuation of the signal before and after it acts in the scattering region. The theoretical assumptions made in the spherical bubble oscillations and nonlinear scattering mechanisms limit the type of sediments for which the method is valid.

Further research in improving the nonlinear acoustic method can be done by exploring a more complex inverse theory of acoustic wave scattering on layered and gas-bearing seafloor.

With the advantages of nonlinear acoustic measuring method, further work can also be done to investigate a more precise relation between the parameters of signal envelopes of both linear and nonlinear responses to the certain types and structures of sediments, since the nonlinear measuring system provides much more information about the surface layer of the sea floor than a single frequency measuring system. With the knowledge of the dependencies between echo signal parameters and acoustic properties of sediments, more investigations can be carried out over large interested areas for a more powerful remote acoustical classification and recognition of the sea floor.

Reference

Anderson, A.L., Hampton, L.D.
Acoustics of gas-bearing sediments I. Background, *J. Acoust. Soc. Am.* Vol. **67**(6), 1865-1889 (1980)

Andreeva, I.B.
Scattering of sound by air bladders of fish in deep sound-scattering ocean layers, Sov. Phys.-Acoust. 10, 17-20 (1964)

Biffard, B., Bloomer, S., Chapman, R.
Single beam seabed classification: direct methods of classification and the problem of slope, Boundary Influence in High Frequency, Shallow Water Acoustics, 227-232, University of Bath, September 2005.

Bachman, R.T.
Acoustic and physical perperty relationships in marine sediment, *J. Acoust. Soc. Am.* Vol. **78**(2), 616-621 (1985)

Blake, F.G.
Spherical wave propagation in solid media, *J. Acoust. Soc. Am.* Vol. **24**, 212-215 (1952)

Boyle, F.A., Chotiros, N.P.
A model for high frequency backscatter from gas bubbles in sandy sediments, *J. Acoust. Soc. Am.* **98**, 531-541 (1995)

Boyle, F.A., Chotiros, N.P.
Nonlinear acoustic scattering from a gassy poroelastic seabed, *J. Acoust. Soc. Am.* **103** (3), 1328-1336 (1998)

Bowles, F.A.
Observations on attenuation and shear-wave velocity in fine-grained, marine sediments, *J. Acoust. Soc. Am.* **101** (6), 3385-3394, June 1997

Brekhovskikh, L.M., Lysanov, Yu.P.

Fundamentals of ocean acoustics, Second Edition, Springer-Verlag, 1991

Didenkulov, I.N.
Measurement of bubble distribution in the subsurface sea layer, XI Session of the Russian Acoustical Society, Moscow, November 19-23 (2001)

Eatock, B.C., Nishi, R.Y., Johnson, G.W.
Numerical studies of the spectrum of low-intensity ultra-sound scattered by bubbles, *J. Acoust. Soc. Am.* Vol. **77**, 1692-1701 (1985)

Emery, K.O., Hoggan, D.
Gases in marine sediments, Amer. Ass. Petrol. Geol. Bull., 42, 2174 (1958)

Eller, A., Flynn, H.G.
Generation of subharmonics of order one-half by bubbles in a sound field, *J. Acoust. Soc. Am.* Vol. **46**, 722-727 (1984)

Eller, A.I.
Damping constant of pulsating bubbles, *J. Acoust. Soc. Am.* Vol. **47**, 1469-1470 (1970)

Gardner, T.
An acoustic study of soils that model seabed sediments containing gas bubbles, *J. Acoust. Soc. Am.* Vol. **107** (1), 163-176, January 2000

Gardner, T.
Modeling signal loss in surficial marine sediments containing occluded gas, *J. Acoust. Soc. Am.* Vol. **113** (3), 1368-1378, March 2003

Kaplan, I.R.
Natural gases in marine sediments, 1974, Plenum Press, New York and London.

Karpov, S.V., Klusek, Z., Marveev, A.L., Potapov, A.I., Sutin, A.M.
Nonlinear interaction of acoustic waves in gas-saturated marine sediments, Acoustical Physics, Vol.42, No.4, 464-470 (1996)

Klusek, Z., Sutin, A., Matveev, A., Potapov, A.I.

Observation of nonlinear scattering of acoustical waves at sea sediments, *Acoustics Letters,* Vol. **18**, No.11 (1995)

Leighton, T.G., Lingard, R.J., Walton, A.J., Field, J.E.
Acoustic bubble sizing by combination of subharmonic emissions with imaging frequency, *Untrasonics* **29**, 319-323 (1991)

Medwin, H., Clay, C. S.
Fundamentals of acoustical oceanography, Academic Press (1998)

Newhouse, V.L., Shankar, P.M.
Bubble size measurement using the nonlinear mixing of two frequencies, *J. Acoust. Soc. Am.* Vol. **46**, 722-727 (1984)

Nyborg, W.L., Rudnick, I., Schilling, H.K.
Experiments on acoustic absorption in sand and soil, *J. Aoust. Sco. Am.* **22**, 422-425 (1950)

Ohsaka, K., Trinh, E.H.
A tewo-frequency acoustic technique for bubble resonant oscillation studies, *J. Aoust. Sco. Am.* **113** (2), 741-749,

Ostrovsky, L.A., Sutin, A.M., Kluzek, Z.
Nonlinear scattering of acoustic waves by natural and artificially generated subsurface bubble layers in sea, *J. Aoust. Sco. Am.* **113** (2), 741-749, February 2003

Ostrovsky, L.A.
Nonlinear, low-frequency sound generation in a bubble layer: Theory and laboratory experiment, *J. Aoust. Sco. Am.* **104** (2), 722-726, August 1998

Ostrovsky, L.A., Sutin, A.M.
Nonlinear acoustic diagnostics of discrete in homogeneities in liquids and solids, 11th Int. Congr. Acoust. Paris, V.**2**, 137-140 (1983)

Prosperetti, A.
Nonlinear oscillations of gas bubbles in liquids: steady-state solutions, *J. Aoust. Sco. Am.* **56** (3), 878-885 (1974)

Richardson, M.D., Briggs, K.B.

Relationships among sediment physical and acoustic properties in siliciclastic and calcareous sediments, Proceedings of the Seventh European Conference on Underwater Acoustics, ECUA 2004, 659-661.

Stoll, R.D.

Anomalous wave velocities in sediments containing gas hydrates, *J. Geophys. Res.* **76**, 2090-2094 (1971)

Stanton, T.K., Clay, C.

Sonar echo statistics as a remote-sensing tool: volume and seafloor, IEEE Journal of Oceanic Engineering, Vol. OE-11, No.1, January 1986

Sternlicht, D.D., Moustier, C.P.,

Remote sensing of sediment characteristics by optimized echo-envelope matching, *J. Aoust. Sco. Am.* **114** (5), 2727-2743 (2003)

Tegowski, J., Jakacki, J., Klusek, Z., Rudowski, S.

Nonlinear acoustic methods in the detection of gassy sediments in the Gulf of Gdansk, Hydroacoustics, Vol.6, 151-158 (2004).

Tegowski, J., Klusek, Z., Jakacki, J.

Nonlinear acoustical methods in the detection of gassy sediments. Acoustic Sensing Techniques for the Shallow Water Environment, 125-136. Springer 2006.

Zabolotskaya, E.A., Soluyan, S.I.

Emission of harmonic and combination frequency waves by air bubbles, *Sov. Phys. Acoust.* Vol. **18**, 396-398 (1972)

Glossary

Absorption The property of a material that changes acoustic energy into (usually) heat energy. A material or surface that absorbs sound waves does not reflect them. Absorption of a given material is frequency dependant as well as being affected by the size, shape, location, and mounting method used.

Attenuation The reduction in amplitude and intensity of an acoustic signal with respect to distance traveled through a medium.

Echo Signal A sound signal reflected off a surface or an object that arrives at the listener after the direct sound.

Far Field That part of the sound field in which sound pressure decreases inversely with the distance from the source, and the angular field distribution is essentially independent of distance from the source.

Fundamental Frequency The fundamental frequency of an oscillating system is the lowest natural frequency of that system.

Hilbert Transform The Hilbert Transform a real-valued signal is obtained by convolving this signal with $1/\pi t$, which is used to describe the complex envelope of real-valued signal.

Hydrophone A sound-to-electricity transducer. Hydrophones are usually used below their resonance frequency over a much wider frequency band where they provide uniform output levels.

Hydrophone Sensitivity The sensitivity of a hydrophone is the minimum magnitude of input acoustic signal required to produce a specified output electrical signal having a specified signal-to-noise ratio, or other specified criteria.

Intensity The power of an acoustic wave per unit area.

Oscillation Variation, usually with time, of the magnitude of a quantity with respect to a specified reference when the magnitude is

	alternately greater and smaller than the reference.
Pressure	The force caused by an acoustic wave per unit area applied on a surface in a direction perpendicular to that surface.
Resonance	The tendency of a system to oscillate with high amplitude when excited by energy at a certain frequency. This frequency is known as the system's natural frequency of vibration or resonant frequency.
Signal Envelope	The variation of the amplitude of an acoustic signal over time.